THE EFFECTS OF CURING REGIMES ON GEOPOLYMER MATERIALS PRODUCED WITH IRON AND STEEL INDUSTRY WASTES

Kinda Ziad ALNAHEEL

2023
MASTER THESIS
CIVIL ENGINEERING

Thesis Advisor
Assoc. Prof. Dr. İlker TEKİN

THE EFFECTS OF CURING REGIMES ON GEOPOLYMER MATERIALS PRODUCED WITH IRON AND STEEL INDUSTRY WASTES

Kinda Ziad ALNAHEEL

Thesis Advisor
Assoc. Prof. Dr. İlker TEKİN

T.C.
Karabuk University
Institute of Graduate Programs
Department of Civil Engineering
Prepared as
Master Thesis

KARABUK
2023

I certify that in my opinion the thesis submitted by Kinda Ziad ALNAHEEL titled "THE EFFECTS OF CURING REGIMES ON GEOPOLYMER MATERIALS PRODUCED WITH IRON AND STEEL INDUSTRY WASTES " is fully adequate in scope and in quality as a thesis for the degree of Master of Science.

Assoc. Prof. Dr. İlker TEKİN
Thesis Advisor, Department of Civil Engineering

This thesis is accepted by the examining committee with a unanimous vote in the Department of Civil Engineering as a Master of Science thesis. 29/11/2023

Examining Committee Members (Institutions)		Signature
Chairman	: Assoc. Prof. Dr. Hacı Süleyman GÖKÇE (BAYU)	(ONLINE)
Member	: Assoc. Prof. Dr. İlker TEKİN (KBU)	
Member	: Assist. Prof. Dr. Mustafa DAYI (DU)	(ONLINE)

The degree of Master of Science by the thesis submitted is approved by the Administrative Board of the Institute of Graduate Programs, Karabük University.

Assoc. Prof. Dr. Zeynep ÖZCAN
Director of the Institute of Graduate Programs

"I declare that all the information within this thesis has been gathered and presented in accordance with academic regulations and ethical principles and I have according to the requirements of these regulations and principles cited all those which do not originate in this work as well."

KINDA ALNAHEEL

ABSTRACT

M. Sc. Thesis

THE EFFECTS OF CURING REGIMES ON GEOPOLYMER MATERIALS PRODUCED WITH IRON AND STEEL INDUSTRY WASTES

Kinda Ziad ALNAHEEL

Karabuk University
Institute of Graduate Programs
Department of Civil Engineering

Thesis Advisor:
Assoc. Prof. Dr. İlker TEKİN
November 2023, 89 pages

Geopolymers and alkali-activated materials are the one of the most common research areas in the construction material science since they are cementless processes. Especially carbon footprint is the main important in cement production, so nowadays industry wastes such as slag, fly ash, metakaolin etc. are triggered to use instead of cement to reduce the negative effects of the cement production to the environment. Alkali-activation is the one of suitable method to be used by binder production. In this study, wastes obtained from the Iron and Steel industry were used in the production of geopolymer materials and the effects of different thermal and environmental curing regimes were tested. Geopolymer materials were prepared with Energy Terminal System ash, Granulated blast furnace slag (GBFS), Ground Granulated blast furnace slag (GGBFS) and MEROS ash sourced from KARDEMIR Iron and Steel Factory. Sodium silicate (Na_2SiO_3) and sodium hydroxide (NaOH) were used in the synthesis of geopolymer materials as alkaline activators. In the research, thermal conditions such as 20±2 °C, 60 °C, 80 °C, 120 °C, 140 °C and 160 °C were created for 1, 2 and 3 hours, and then the effect of environmental conditions, including dry and humid environments, was also examined.

In the experimental study, workability, compressive strength, and water absorption tests were performed. Moreover, mineralogical, and microscopic analyses were conducted by XRD and SEM+EDS methods, respectively. Fresh state properties were assessed through a flow table test, providing insights into the workability of geopolymer material. The hardened state properties were examined through compressive strength and water absorption tests conducted on the 2^{nd} and 28^{th} days.

The maximum compressive strength for the Geopolymer pastes at 28 days was achieved on the GGBFS-based GPs as 46.9 MPa, using an 80°C temperature and 2-hour oven curing. The minimum compressive strength values were obtained on the GBFS-based GPs. In the SEM images, geopolymer forms were observed in the Geopolymer pastes.

Key Words : Geopolymer paste, ground granulated blast furnace slag, steel slag, energy terminal system ash, sinter ash, different curing regimes.

Science Code :91127

ÖZET

Yüksek Lisans Tezi

DEMİR ÇELİK ENDÜSTRİSİ ATIKLARI KULLANILARAK ÜRETİLEN JEOPOLİMER MALZEMELER ÜZERİNDE KÜR REJİMLERİNİN ETKİLERİ

Kinda Ziad ALNAHEEL

Karabük Üniversitesi
Lisansüstü Eğitim Enstitüsü
İnşaat Mühendisliği Anabilim Dalı

Tez Danışmanı:
Doç. Dr. İlker TEKİN
Kasım 2023, 89 sayfa

Jeopolimerler ve alkali-aktive malzemeler, çimentosuz prosesler olmaları nedeniyle yapı malzemesi biliminin en yaygın araştırma alanlarından biridir. Özellikle karbon ayak izi çimento üretiminin önemli bir parçası olması sebebiyle, günümüzde çimento üretiminin çevreye olumsuz etkilerini azaltmak amacıyla cüruf, uçucu kül, metakaolin gibi endüstri atıklarının çimento yerine kullanılması talep edilmektedir. Alkali aktivasyon, bağlayıcı üretimi için kullanılabilecek uygun bir yöntemlerden biridir. Bu çalışmada Demir Çelik endüstrisinden elde edilen atıklar geopolimer malzeme üretiminde kullanılmış ve farklı ısıl ve ortam kür rejimlerinin etkileri denenmiştir. Geopolimer malzemeler, Kardemir Demir Çelik Fabrikası'ndan temin edilen Enerji Terminal Sistemi külü, Granül yüksek fırın cürufu (GBFS), Öğütülmüş Granül yüksek fırın cürufu (GGBFS) ve MEROS külü ile hazırlanmıştır. Jeopolimer malzemelerin sentezinde alkali aktivatör olarak sodyum silikat (Na2SiO3) ve sodyum hidroksit (NaOH) kullanılmıştır. Araştırmada 1, 2 ve 3 saatlik süreçlerde 20±2 °C, 60 °C, 80 °C, 120 °C, 140 °C ve 160 °C gibi ısıl koşullar oluşturulmuş ve ardından kuru ve nemli ortamlar olmak üzere çevresel koşulların etkisi de incelenmiştir.

Deneysel çalışmada işlenebilirlik, basınç dayanımı ve su emme testleri yapılmıştır. Ayrıca mineralojik ve mikroskobik analizler sırasıyla XRD ve SEM+EDS yöntemleriyle yapılmıştır. Taze durum özellikleri, jeopolimer malzemenin işlenebilirliği hakkında bilgi sağlayan bir akış tablosu testi aracılığıyla değerlendirildi. Sertleşmiş hal özellikleri 2. ve 28. günlerde yapılan basınç dayanımı ve su emme testleri ile incelenmiştir.

Geopolimer macunların 28 günde maksimum basınç dayanımı, GGBFS bazlı GP'lerde 80°C sıcaklık ve 2 saatlik fırında kürleme kullanılarak 46,9 MPa olarak elde edildi. Minimum basınç dayanımı değerleri GBFS tabanlı GP'lerde elde edildi. SEM görüntülerinde Geopolimer macunlarda geopolimer formları gözlendi.

Anahtar Kelimeler : Geopolimer hamuru, toz halinde yüksek fırın cürufu, çelik cürufu, enerji terminali sistemi külü, sinter külü, farklı iyileştirme rejimleri.

Bilim Kodu :91127

ACKNOWLEDGMENT

Foremost, to be able to thank Allah is a blessing within itself. Thanks to Allah for everything even the trials that makes me able to complete and finish my thesis successfully.

I would like to express my deepest gratitude to my supervisor, Assoc. Prof. Ilker Tekin, who gave me his idea, topic of this thesis, planning of the experimental study, design of the geopolymer pastes and the opportunity to do this research. I am grateful to him for his continuous support, patience, guidance and wide knowledge. I appreciate it all. Besides my advisor, I would like to thank the rest of my thesis committee, and also, my fellow lab mates.

Last but not the least, I wanted to reach out and express my thanks to my family for all the support. Finally, thanks for all those supported me directly or indirectly.

CONTENTS

Page

APPROVAL ii
ABSTRACT iv
ÖZET vi
ACKNOWLEDGMENT viii
CONTENTS ix
LIST OF FIGURES xii
LIST OF TABLES xiii
SYMBOLS AND ABBREVITIONS INDEX xiv

PART 1 1
INTRODUCTION 1
1.1. GENERAL 1
1.2. THESIS SCOPE, AIM, AND OBJECTIVES 3
1.2.1. Subject and Scope 3
1.2.2. Aim and objective 3
1.2.3. Objective 3
1.3. THESIS ARRANGEMENT 4

PART 2 5
LITERATURE REVIEW 5
2.1. ASSESSMENTS ON BINDING MATERIALS 5
2.2. GEOPOLYMER MATERIALS 6
2.2.1 History of Geopolymer Materials 6
2.2.2. Mechanism Of Geopolymeric Binders 8
2.2.3. Alkali-activated concrete (AAC) 11
2.2.4. Components of Geopolymer Materials 11
2.2.4.1. Sodium Hydroxide (NaOH) 14
2.2.4.2. Sodium Silicate (Na2SiO3) 15

Page

2.2.4.3. Dosage of activators 15
2.2.5. Curing of Geopolymer 17
2.2.6. Advantages and Disadvantages of Geopolymer 19
2.3. LITERATURE REVIEW 20

PART 3 31
MATERIALS AND METHODS 31
3.1. MATERIALS 31
3.1.1. Granulated Blast Furnace Slag (GBFS) 31
3.1.2. Ground granulated blast furnace slag (GGBFS) 32
3.1.3. Steel Slag 34
3.1.4. Energy Terminal System Ash (EPA) 35
3.1.5. MEROS Ash (Sinter Ash) 36
3.1.6. Alkaline Activators 38
3.2. EXPERIMENTAL METHODS 39
3.2.1. Preparing of Geopolymer Pastes 39
3.2.2. Curing Process 40
3.2.3. Experimental Studies 42
3.2.3.1. The Flow Table Test On Fresh State Geopolymer Materials 42
3.2.3.2. The Compressive Strength Test On Hardened State Geopolymer Materials 43
3.2.3.3. The Water Absorption Test On Hardened State Geopolymer Materials 44

PART 4 46
RESULTS AND DISCUSSION 46
4.1. FLOW TABLE TEST RESULTS AND DISCUSSIONS 46
4.2. THE UNIT WEIGHTS RESULTS AND DISCUSSIONS 47
4.3. THE COMPRESSIVE STRENGTH TEST RESULTS AND DISCUSSIONS 50
4.4. WATER ABSORPTION TEST RESULTS AND DISCUSSIONS 55
4.5. MICROSTRUCTURAL AND MINERALOGICAL ANALYSES 61

Page

4.5.1. SEM Analyses 61
4.5.2. XRD Analyses 67

PART 5 69
SUMMARY AND CONCLUSIONS 69
5.1. GENERAL 69
5.2. CONCLUSION 69
5.3. SUGGESTED RECOMMENDATIONS FOR FUTURE STUDIES IN THIS FIELD 71
REFERANCES 73

ADDITIONS 83

CURRICULUM VITAE 89

LIST OF FIGURES

Page

Figure 2.1. Classification of Geopolymer cement [16]..... 6

Figure 2.2. Development of the Geopolymerization Process on a Conceptual Level [28]. 9

Figure 2.3. Hardening of Portland cement and geopolymer cement [30]. 10

Figure 2.4. Elemental compositions measured for gel regions in a 1:1 fly ash: blast furnace slag binder activated by Na_2SiO_3 solution, at ages of 28, 90 and 180 days [51]. 14

Figure 2.5. Variation ratio of SiO2 to Na2O in the early compressive strength of AAMs" (Hussein et al., 2016) [60]. 16

Figure3.1. a) GBFS, b) GGBFS. 32

Figure3.2. SEM image and XRD pattern of GGBFS [101]. 33

Figure3.3 SEM images and XRD pattern of EPA [101]. 34

Figure3.4. a) SS above the 2 mm sized sieve, b) SS after the sieving process, c) EPA 35

Figure3.5. SEM images and XRD pattern of EPA [101]. 35

Figure3.6. Particle size analysis of GGBFS and EPA [101]. 36

Figure3.7. Meros Ash 37

Figure3.8. XRD analysis and SEM images of SA [101] 37

Figure3.9. Sodium Silicate (Na2SiO3) and 10 M of NaOH liquid 38

Figure3.10. The scheme of the experiments 42

Figure3.11. Spreading table and spreading diameter measurement. 43

Figure3.12. Compressive strength test machine 43

Figure3.13. Representation of water absorption test steps 45

Figure 4.1. flow table test procedure 46

Figure 4.2. Unit weights of the GBFS-based GPs for a) ambient at 2^{nd} day, b) wet curing at 2^{nd} day, c) ambient at 28^{th} day and d) wet curing at 28^{th} day.... 47

Figure 4.3. UW of GGBFS-based GPs for a) Ambient, b) Wet curing conditions at 2^{nd} day. c) Ambient, d) Wet curing conditions at 28^{th} day. 49

Figure 4.4. Compressive Strength (MPa) values of GBFS-based GPs at 28^{th} day. ... 51

Figure 4.5. Compressive Strength (MPa) values of GGBFS-based GPs for ambient curing and wet curing conditions at 2^{nd} day. 53

Page

Figure 4.6. Compressive Strength (MPa) values of GGBFS-based GPs for ambient curing and wet curing conditions at 28th day. 54

Figure 4.7. Water Absorption (%) values of GBFS-based GPs for ambient curing and wet curing conditions at 28th day. 56

Figure 4.8. Apparent Porosity (%) values of GBFS-based GPs for ambient curing and wet curing conditions at 28th day. 57

Figure 4.9. Water Absorption (%) values of GGBFS-based GPs for ambient and wet curing conditions at 28th day. 58

Figure 4.10. Apparent Porosity (%) values of GGBFS-based GPs for ambient and wet curing conditions at 28th day. 59

Figure 4.11. GBFS-Wet samples at 140 °C before immersing in water 60

Figure 4.12. SEM images and EDS spectrum of Reference GGBFS-based GP in wet curing 61

Figure 4.13. SEM images and EDS spectrum of reference GGBFS-based GP in wet curing in the laboratory. 62

Figure 4.14. SEM images and EDS spectrum of reference GGBFS-based GP in ambient curing 63

Figure 4.15. SEM images and EDS spectrum of GGBFS-based GP 80 ºC-3h curing in ambient curing 64

Figure 4.16. SEM images and EDS spectrum of GGBFS-based GP 120 ºC-2h curing in ambient curing 65

Figure 4.17. SEM images and EDS spectrum of GGBFS-based GP 160 ºC-2h for ambient curing. 66

Figure 4.18. XRD analysis of materials used in GPs. 67

Figure 4.19. XRD analysis of produced GPs. 68

LIST OF TABLES

Page

Table 2.1. Alkali Activated Cements timeline [21] 7
Table 2.2. Alkaline types of cement and its properties [31]. 10
Table 2.3. Wastes derived from iron/steel making [44]. 12
Table3.1. The physical properties of all solid components. 32
Table3.2. The chemical properties of components. 33
Table3. 3 Semi-Quantitative Phase Analysis Results with XRD (mg/kg). 37
Table3.4. Metal Analysis Results. 38
Table3.5. The chemical and physical properties of Na_2SiO_3 [102]. 39
Table3.6. Mix design of geopolymer materials (by weight). 40
Table3.7. Study design of Material-based GPs specimens. 41
Table 4.1. Compressive Strength and unit weights of GBFS geopolymer paste. 50
Table 4.2. Compressive Strength and unit weights of GGBFS geopolymer paste. ... 53
ADDITIONS
Table 1. The breakdown forms patterns and cracks after the compressive strength test for GGBFS and GBFS samples at 60°C 83
Table 2. The breakdown forms patterns and cracks after the compressive strength test for GGBFS and GBFS samples at 80°C. 84
Table 3. The breakdown forms patterns and cracks after the compressive strength test for GGBFS and GBFS samples at 120°C. 85
Table 4. The breakdown forms patterns and cracks after the compressive strength test for GGBFS and GBFS samples at 140°C. 86
Table 5. The breakdown forms patterns and cracks after the compressive strength test for GGBFS and GBFS samples at 160 °C. 87
Table 6. The breakdown forms patterns and cracks after the compressive strength test for GGBFS and GBFS reference samples. 88

SYMBOLS AND ABBREVITIONS INDEX

SYMBOLS

%	: Percent Sign
^{o}C	: Degrees Celsius
m	: Meter
cm	: Centimeter
mm	: Millimeter
Min	: Minute
s	: Seconds
Kg	: Kilogram
NaOH	: Sodium Hydroxide
Na_2SiO_3	: Sodium Silicate
CO_2	:Carbon Dioxide

ABBREVITIONS

GPC : Geopolymer Concrete
GPs : Geopolymer Pastes
AAM : Alkali Activated Material
AAFA : Alkali-Activated Fly Ash
AAS : Alkali Activated Slag
AAC : Alkali-Activated Concrete
OPC : Ordinary Portland Cement
FA : Fly Ash
GGBS : Ground Granulated Blast-Furnace Slag
GBS : Granulated Blast-Furnace Slag
C-S-H : Calcium Silicate Hydrate
AASCC : Alkali-Activated Slag Cement and Concrete
ASTM : American Society for Testing and Material
XRD : X-ray diffractometers
SEM : Scanning electron microscope

PART 1

INTRODUCTION

1.1. GENERAL

Portland cement (PC) is one of the main components of concrete and represents 10-12% of the total concrete volume, PC also one of the most widely used building materials, with an average consumption of 1 ton/year per person [1]. In addition to the negative impact of greenhouse gas emissions, which leads to a global warming [1]. It is well known that the production of ordinary PC is one of the largest sources of carbon dioxide emissions into the atmosphere. This is the main motive to produce building materials with lower environmental impacts [2]. The ever-increasing demand for cement and concrete, the depletion of fossil fuel reserves, the scarcity of raw materials, and the growing environmental concerns associated with climate change are some of the biggest challenges facing the cement industry [3]. The problem of energy consumption in the cement industry is the main problem that has recently led to an increase in the energy crisis in the world and it is restricting development. Therefore, sustainable development methods in binding materials will be research for the use of iron and steel wastes such as Blast Furnace Slag (BFC), and Steel Slag (SS) [4]. And due to the increasing demand for building materials, this has led to a significant increase in its production, reaching around 3 billion tons globally, and it is expected to reach 6 billion in the coming years [1]. In addition to the increase in the global warming due to the negative effects resulting from the manufacture of concrete [1]. Waste in general make threats against human health and the natural environment with varying effects. Because of the rise in the amount of industrial waste leads to serious problems at the global and local levels, so waste management has become one of the most important contemporary issues. The goal of waste management is to reduce waste and dispose it appropriately [5].

Because of the great technical progress in the past few years there has been development of new materials such as “Geopolymers” as new materials with unique and highly desirable chemical and mechanical properties, and new technologies for

their use, these newly designed new materials with the help of geopolymerization reactions present new fields and procedures [6]. It is strongly believed that the process of sustainable development of the metals and steel sector using metal and mining waste contributes to the improvement and development of the geopolymerization process and thus the stabilization of hazardous waste and the synthesis of geopolymers with advanced properties. Geopolymers can be made when naturally occurring materials are mixed with sodium hydroxide and water for this reason, they are relatively inexpensive to produce [7]. Source materials such as fly ash used during the installation of geopolymers have a significant role in determining the final properties of the geopolymer matrix [8]. In a short period of time, geopolymers have shown great potential to be used as a cement due to its contribution to reducing the negative environmental effects of CO_2 [8].

Due to the ever-increasing CO_2 emissions in the cement industry, attentions now focus on research interest in reducing these emissions. Alkaline activated materials (AAM) and Geopolymers produced by fly ash, BFS and silica fume have become an important research topic [9]. Where it has become possible to take advantage of iron and steel industry wastes and sampling to identify its characteristics and optimal use [10]. Geopolymer concrete has good physical properties and a positive impact on the environment compared to the traditional concrete. Where OPC can be completely replaced by fly ash and alkaline active binders with the aim of making concrete less energy consuming and more environmentally friendly [10]. Using geopolymer concrete aims to study the combined effect of curing conditions and the use of fly ash as a raw material on the compressive strength of geopolymer concrete. in addition to the use of a mixture of sodium hydroxide and sodium silicate as an alkaline activator. The general aim of geopolymer concrete curing is to identify the impact and compare the effects of different curing conditions on the physical, mechanical, and microstructural properties of manufactured specimens. Studies have found that oven-cured specimens is more efficient compared to other types of curing.

The different curing conditions have an impact on the physical, mechanical, and microstructural properties of samples created from geopolymer paste. Experimental results have shown a distinct effect of curing on geopolymer mixtures. In ambient-

cured specimens, the density, Poisson's ratio, and drying shrinkage were higher compared to oven-cured specimens. Conversely, the oven-cured specimens exhibited higher elasticity modulus, tensile strength, and compressive strength.

1.2. THESIS SCOPE, AIM, AND OBJECTIVES

1.2.1. Subject and Scope

There is no study in this area examining Steel slag and GGBFS based AAM and geopolymers made by MEROS Sinter ash (SA) and Energy Terminal System ash (ETSA). Therefore, the purpose of this research is to create a new GBFS and GGBFS based geopolymer binding material with SA and ETSA and by combining various of temperatures and hours.

1.2.2. Aim and objective

This thesis aims to make different types of slags based geopolymer and investigate the effect on the Mechanical properties when SA are added to the mixes using a variety of temperatures so as to improve the workability that results in a high compressive strength.

1.2.3. Objective

- To obtain higher compressive strength and water resistance of hardened geopolymers using SA and ETSA at various temperatures.
- To produce a cost-efficient geopolymer mixture to improve the processing of geopolymers.
- To obtain the microstructure of new geopolymer mortars without PC.
- To investigate the impact of curing conditions, specifically ambient curing and oven-curing, on the physical, mechanical, and microstructural properties of the specimens.

1.3. THESIS ARRANGEMENT

As for the rest of the thesis, it is set up as follows:

Part 2: Background of the AAM and geopolymers and most used additives and admixtures worldwide.

Part 3: Illustrates the approach done to produce the pastes and the test applied in the fresh and hardened pastes.

Part 4: Illustrates and discusses the tests results.

Part 5: The conclusion part and the summary of this study based on the results

PART 2

LITERATURE REVIEW

2.1. ASSESSMENTS ON BINDING MATERIALS

Today, construction activity is increasing rapidly to meet the needs of ever-growing infrastructure. Cement-based concrete proves to be an essential and very widely used material in most construction activities. The annual consumption of concrete throughout the world approaches 20,000 million metric tons in 2009 [11]. Approximately 8% of global CO_2 emissions arise from the cement manufacturing. However, the cement manufacturing process releases kind of large amounts of CO_2 into the atmosphere through fuel consumption and raw material conversion. Producing 1 ton of Portland clinker directly produces 0.55 ton of chemical CO_2 and needs burning carbon fuel to produce another 0.40 ton of CO_2, hence: 1t of PC = 0.95t of CO_2 [12].

Researchers have specifically put a very large effort to find a solution to gradually reduce this energy consumption and partially replace cement with other environmentally friendly materials, which for the most part is quite significant [13]. Contrastingly, the amount of industrial waste generated such as fly ash from thermal power plants, slag from steel production, mine tailings from mining plants, red mud from the alumina industry, and basalt pumice from the ceramics industry has increased significantly [14,15]. Fly ash can be classified by ASTM C 618 into two classes depending on the coal-components as class F and class C fly ash [63].

Recently, the studies about the binding materials tend to the cementless binding systems [15]. Lastly patented by Davidovids called as "geopolymer" systems are used as a general descriptor for an amorphous alkali-aluminosilicate material. Geopolymers include aluminum silicate binder, alkalis, and aggregates as fillers,

while the additional components may involve water, additives, and fibers etc. [16]. Geopolymer concrete can be produced by polymerizing aluminum silicates through alkaline activation method, as it can be seen in Figure 2.1.

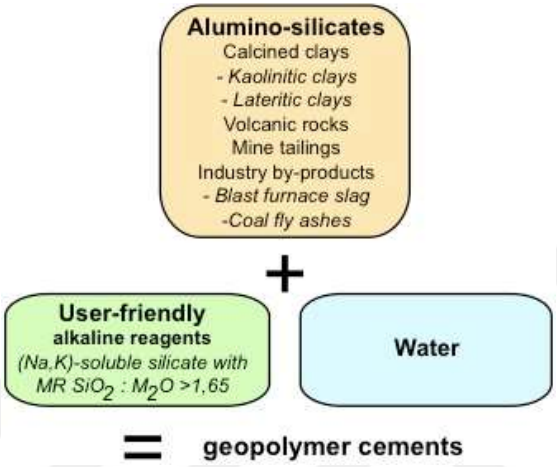

Figure 2.1. Classification of Geopolymer cement [16]

2.2. GEOPOLYMER MATERIALS

2.2.1 History of Geopolymer Materials

Alkali as a component of cementitious materials was first used in 1930 as Kuhl examined the hardening behavior of mixtures of a mixture of powdered slag and potassium hydroxide (KOH) solution. Amongst several studies that have been conducted after that to clarify the effects of alkali on future cementitious systems, Purdon has accomplished an essential one in 1940 when he spread the first large-scale study of clinker-free cements [17]. This has led to extensive research and development of alkali-activated cements and concretes. These cements have just latterly begun to obtain real technological noteworthiness although in 1982 Davidovits mixed alkalis with a calcined mixture of kaolinite, limestone, and dolomite to produce a binder [18].

Simultaneously, the steadily expanding understanding of alkali-activated cements and concretes has illuminated their advantages with respect to decreased energy costs and their impact on the environment, as well as their excellent physical properties [19-20],

and sufficient durability [21,22]. The most important and influential studies on alkaline cement are summarized by Palomo Et al. as shown in Table (2.1).

Table 2.1. Alkali Activated Cements timeline [21]

Year	Name	Study/Impact
1930	Kühl	Slag setting in the presence of dry potash
1937	Chassevent	Slag reactivity measurement using a dry potash and soda solution
1940	Purdon	Clinker-free cements consisting of slag and caustic soda or slag and caustic alkalis synthesised with a base and an alkaline salt
1957	Glukhovsky	Binder synthesis using hydrous and anhydrous aluminosilicates (vitreous rocks, clays, steel mill slag) and alkalis; proposal for a Me_2O-MeO-Me_2O_3- SiO_2-H_2O cementitious system; coining of the term "soil cement"
1981	Davidovits	Alkalis mixed with a blend of burnt kaolinite, limestone and dolomite, and trademarks such as Geopolymer, Pyrament, Geopolycem, Geopolymite
1986	Krivenko	Principles governing system Me_2O-MeO-Me_2O_3-SiO_2-Al_2O_3 properties; proposal for the generic name "alkaline cements" and the specific name "geocement"
1999	Palomo	Production of hardened cementitious materials from alkali-activated type F fly ashes
2006	Shi & Krivenko & Roy	First book on alkali-activated cements
2014	Provis J., & van Deventer J.S.J	Alkali activated Materials State of the art Report. RILEM TC 224-AAM

Alkali-activated cements is divided into five groups based on the composition of the cementitious components as criteria [23]:

1. Alkali-activated slag-based cements.

The most extensively studied system in the 1980s and 90s was alkali-activated blast furnace slag cement. Its major properties are as follows:

The type of slag and the type and dosage of the used activator are the two features that most affect this binder's performance. The type of the activator determines whether alkali-activated slag cement pastes and mortars are more porous or less than OPC

pastes and mortars. OPC and concrete resist caustic environments like acids, and chlorides less than alkali-activated slag cement and concrete [23].

In all cases, the main reaction produces a C-S-H gel which contains aluminium in its texture [23]. There is no releasing of Ca $(OH)_2$, therefore, alkali-activated slag paste provides fire resistance more efficiently than OPC. Conversely, the ratio of Ca/Si and the amount of Al in the gel depending on the properties of the activator, the chemical structure of the cementitious ingredient, and curing restriction (time and temperature).

2. Alkali-activated pozzolan cements. Include several cementitious systems as follows:
    - Alkali-activated fly ash cement.
    - Alkali-activated natural pozzolan cement.
    - Alkali-activated metakaolin cement.
    - Alkali-activated soda lime glass cement.
3. Alkali-activated lime-pozzolan/slag cements.
4. Alkali-activated calcium aluminate blended cements.
5. Alkali-activated Portland blended cements (hybrid cements).

2.2.2. Mechanism Of Geopolymeric Binders

Geopolymers are manufactured by dissolving an aluminosilicate oxide in an alkaline solution, which is usually a concentrated alkali hydroxide such as NaOH, KOH, and alkali silicates such as Na_2SiO_3, K_2SiO_3 [24]. The mechanism of forming geopolymers is called repolymerization and involves the following three steps: Dissolution, transportation / orientation / condensation, and polycondensation [25]. Which agrees with the proposal of the polymerization model of Glukhovsky: destruction–coagulation, coagulation-condensation, condensation– crystallization. When alkaline activator is added to the raw material, the silicates and aluminates dissolve and cause an ionic junction between Al and Si parts, and then a covalent bonding with oxygen molecules takes place to generate precursor ions. The range of dissolution requires oxide synthesis of the raw materials and the activator concentration. Subsequently, these ions of the precursors are adjusted and condensed to produce a monomer. These

monomers are then polycondensed to produce rigid 3D structures of silicates and aluminates as given in Eq. 2.1 [26].

During the coagulation-condensation phase, a hydroxyl complex is formed within the Si-O-Si bonds. This complex subsequently undergoes condensation, resulting in the formation of fresh Si-O-Si bonds and the generation of dimers. The ultimate phase of polymerization and solidification dictates the microstructure and distribution of pores within the cured geopolymer. [27]. As shown in Figure 2.2 Subjected to alkali attack, raw material dissolves. Monomers aggregate, forming larger entities. Initially, Gel 1 forms with Si/Al ratio, Gel 2 hosts polymerization, yielding substantial molecular reaction products [28].

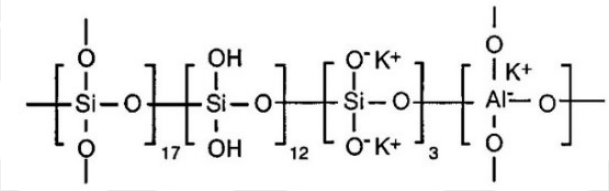

Eq. 2.1. Synthesis and Characterization of rigid 3D structures of silicates and aluminates [27].

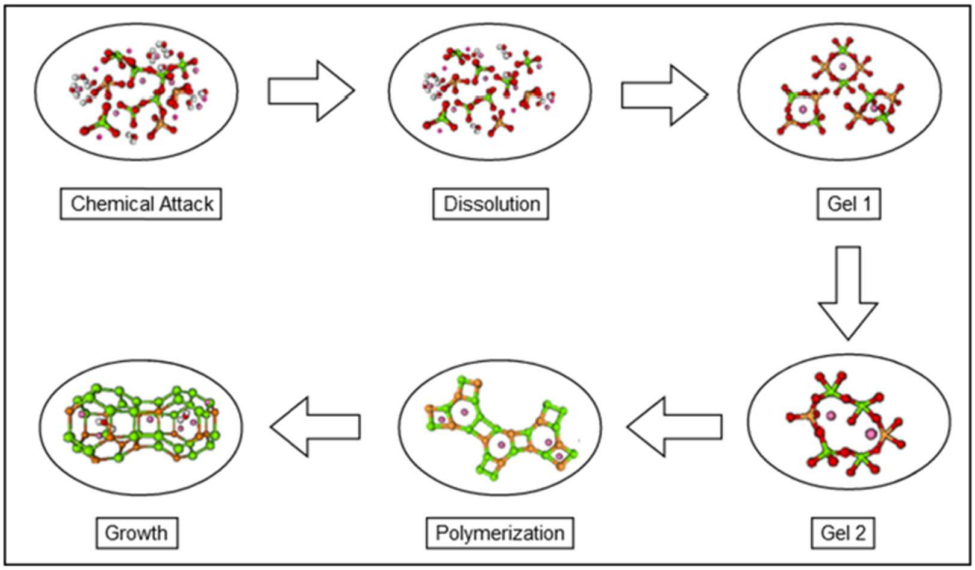

Figure 2.2. Development of the Geopolymerization Process on a Conceptual Level [28].

In recent years, geopolymers have received much attention among other binders due to their initial compressive strength, low permeability, excellent chemical resistance, and really good fire resistance performance [29]. In contrast to the cement hydration, geopolymer cement hardens through polycondensation of potassium oligo-(sialate-siloxo) into crosslinked potassium-poly(sialate-siloxo) networks as described in Figure 2.3 [30].

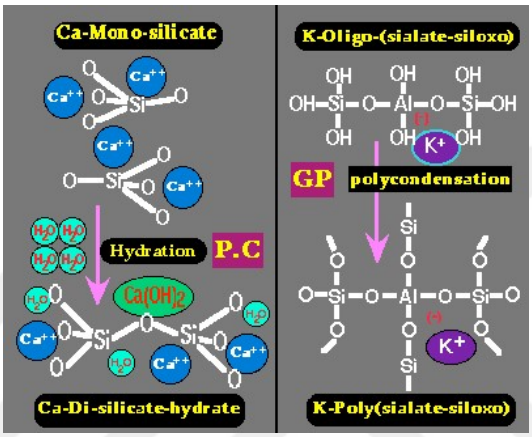

Figure 2.3. Hardening of Portland cement and geopolymer cement [30].

Alkaline-activated cements and concretes exhibit better mechanical results than OPC because of their properties (Table 2.2). Alkaline types of cement can be separated into two groups based on the characteristics of the cementitious components ($CaO–SiO_2–Al_2O_3$) where Type 1: high calcium oxide content, Type 2: low calcium cements [31].

Table 2.2. Alkaline types of cement and its properties [31].

Model	Alkaline Activity	Properties	Ref.
Type1 (C-A-S-H)	$(Na,K)_2O–CaO–Al_2O_3$-$SiO_2–H_2O$	Activated under relatively moderate alkaline conditions	[31-32]
Type2 (N-A-S-H)	$(Na,K)_2O–Al_2O_3$-–$SiO_2–H_2O$	Materials activated comprise primarily aluminum and silicon such as metakaolin or fly ash. Materials have low CaO contents. More aggressive working conditions to kick-start the reaction	[33-34]
Type3 ((N,C) A-S-H)	Combination Type1 and Type2	CaO, SiO_2 and Al_2O_3 contents > 20%.	[35-36]

2.2.3. Alkali-activated concrete (AAC)

Alkali-activated concrete (AAC), also known as geopolymer concrete, is an environmentally conscious building material that offers an alternative to the conventional Portland cement-based concrete [36]. AAC derives its name from the activation process, which involves the use of alkaline solutions instead of Portland cement as the binding agent. This innovative approach yields concrete with comparable or even superior characteristics to traditional options, delivering benefits such as diminished carbon emissions and reduced energy consumption during manufacturing [37]. source materials, including fly ash, slag, metakaolin, and industrial waste products that are rich in alumina and silica, are essential for the formation of the geopolymer binder. The activation procedure entails blending source materials with alkaline activators, typically sodium hydroxide (NaOH) and sodium silicate (Na2SiO3). This combination initiates a chemical reaction that culminates in the creation of a robust and long-lasting material through covalent bonds. The primary advantage of AAC lies in its diminished environmental impact in comparison to traditional cement-based concrete. It necessitates less energy for production and can incorporate industrial waste, consequently reducing the carbon footprint associated with cement manufacturing [39].

2.2.4. Components of Geopolymer Materials

Pozzolanic materials are siliceous and aluminous materials that have little or no cementitious properties intrinsically, and they chemically react with calcium hydroxide Ca (OH)2 at average temperatures when situated in a water-containing form that divided meticulously, this process leads to producing compounds with cement-like properties [37]. Pozzolanic activity assesses the pozzolanic ability to react with water and calcium hydroxide [38]. Basically, the slow pozzolanic reaction decelerates the generation of heat of hydration and the progression of strength. This reaction requires the consumption of Ca(OH)2; therefore, no Ca(OH)2 is produced. The mitigation of Ca (OH)2 enhances the durability of cement mortars by densifying them and turning them impermeable [39].

Pozzolanic materials are divided into two groups: Natural (Calcined diatomaceous earths, volcanic ash, tuffs, pumice, opaline cherts, clay and shales) and artificial (man-made) (Silica fume, fly ash, blast furnace slag). Artificial pozzolans can be created intentionally in several ways, e.g., by activating kaolin clay thermally to get metakaolin, or from high-temperature processes that generate wastes or by-products, like fly ash produced during the burning of coal to generate power [40].

Pozzolanic materials in alkali-activated cement and concrete, various by-products and industrial wastes in addition to many aluminosilicates raw materials are used. These materials could be granulated phosphorus slag, granulated blast furnace slag, steel slag [41]. Volcanic glass is a natural glass formed from rapidly cooling lava. Tuff, on the other hand, is a rock made from compacted volcanic ash and fragments. It forms layers after explosive volcanic eruptions. Both volcanic glass and tuff offer insights into past volcanic activity and landscape history [42].

Making iron or steel produces give rise to many wastes, and these are shown in Table 2.4. The main kind of waste generated from steel production according to the volume is slag which has been considered a beneficial by-product, not just a waste substance. There is a variety of slag types. Flue dust and refractory linings from furnaces are as well considerable waste types [43].

Table 2.3. Wastes derived from iron/steel making [44].

Process	Raw materials	Wastes/by-products
Iron smelting	Iron ore, Limestone, Coke, Air	Blast furnace slag, Flue dusts, Ash, Refractory linings
Steel making	Pig iron and/or steel and iron scrap	Steel slag, Flue dusts, Refractory linings
Iron casting	Pig iron, Coke, Moulding sand	Foundry slag, Moulding sand
Processing of steel	Crude steel	Spent acids and alkalis, hydroxide, sludges, spent plating solutions, mill scale, oils, solvents, paints, non-ferrous metals

There are three main forms of slag depending on the average and method of cooling down the molten slag coming out from the blast furnace: Air cooled, foamed or expanded, granulated. Some problems with using the blast furnace slag are related to the sulfur content of the slag itself which comes out from the coke used in the furnace. High concentricity of water-soluble sulfates can lead to the origination of sulfoaluminates like ettringite (3CaO.Al2O.3CaSO4.30-32H2O). This secondary mineral formation is associated with a volume expansion of around about 120% and moreover can lead to ground uplift. Furthermore, high concentration of sulfate can as well cause a chemical attack of concrete [45,46].

Jiang 1997 [47] defined alkali activation as the way of using alkaline ions to generate pozzolanic reactions and liberate potential cementitious features of inorganic materials that superbly divided. The chemical composition of the alkaline activator considerably affects precursors. Alkali activation takes place when the industrial by-products are activated by a mixture of industrial products that are readily available to support new implementations because they are manufactured in large quantities and their manufacturing techniques are ubiquitous, which are called activators. The most used activators are Sodium Hydroxide (NaOH), 98% pure flakes, with Sodium Silicate (Na2SiO3) or Potassium Hydroxide (KOH). The classes of sodium silicate solution are varied and defined by their silica modulus or SiO2/Na2O ratio, while the electrolysis of sodium chloride solution forms a solid NaOH that dissolves in water providing a solution with wanted molarity [48]. Alkali activators have an essential function in hydrating binders. Glukhovsky et al. [49] assorted the alkaline activators into 6 groups as claimed by their chemical composition: caustic alkalis, nonsilicate strong and weak acid salts, and aluminosilicates.

Most studies established that the activation with sodium silicate causes better strength. Wang et al. found that the type of activator affects the strength of AAS and that using a liquid form of sodium silicate causes higher performance than using powder shape [50]. Moreover, the amount of calcium is one of the major features to take into account in the precursor materials. Ismail et al., 2014, studied the differences of calcium content and their effects at different curing ages of binders, and found that C–A–S–H

gel become more homogeneous with longer-term curing, while N–A–S–H gel keep more constant (Figure2.4) [51].

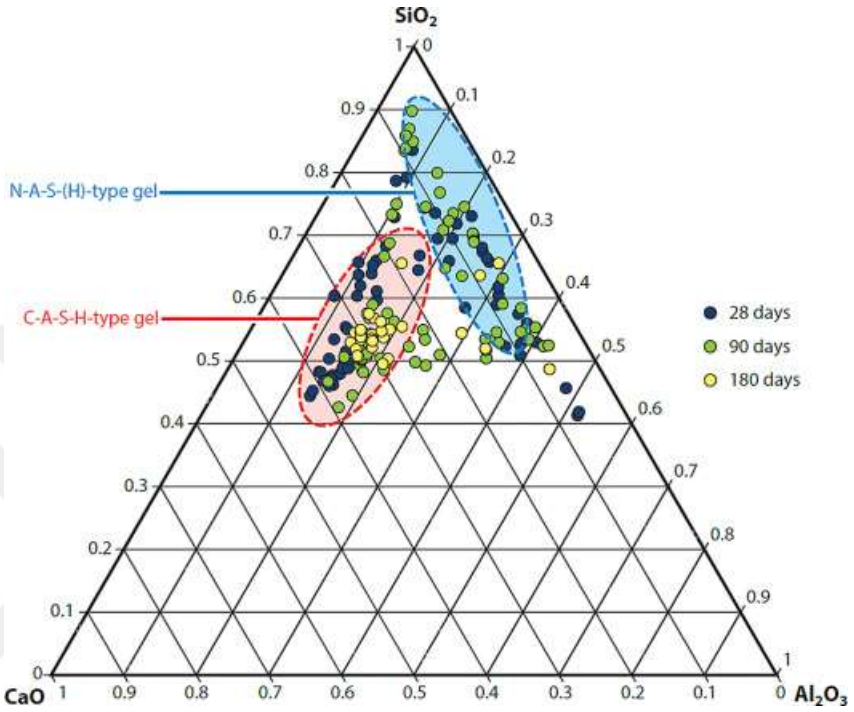

Figure 2.4. Elemental compositions measured for gel regions in a 1:1 fly ash: blast furnace slag binder activated by Na_2SiO_3 solution, at ages of 28, 90 and 180 days [51].

2.2.4.1. Sodium Hydroxide (NaOH)

Sodium hydroxide is highly alkaline and binds highly with water. Sodium hydroxide (caustic soda) is a potent alkaline compound (NaOH) Sodium hydroxide is one of the most important industrial chemicals and a powerful moisture absorbent, used widely in various industries: chemicals, paper, textiles, and water treatment. Also used in alumina refining to separate aluminium from impurities. [52].

Sodium hydroxide comes in different forms in industries, while it is not directly natural-sourced also it is a powerful source of bases in industry. Approximately 56 % of sodium hydroxide is produced by the dissolved industry which produced from salt electrolysis or mineral extraction. The most common type is solid sodium hydroxide. [53]. It exists as a white solid or thick liquid. Sodium hydroxide is a highly caustic and

reactive substance and should be handled with care. This makes sodium hydroxide extremely corrosive, damaging to the skin, burns a lot and decomposes quickly in water, which generates a lot of heat. It's often used as a solution in water, and protective equipment, such as gloves and goggles. The exact usage depends on the specific application, but it's generally added slowly to water while stirring to avoid splattering [54].

2.2.4.2. Sodium Silicate (Na_2SiO_3)

Sodium silicate, also called soluble glass or water glass, is a compound containing (Silicon Dioxide, Sodium Silicate Na_2SiO_3) which are mixed in a certain proportion, as the increase of one of the two oxides over the other leads to completely different use. It is produced by fusing silica sand (SiO_2) with sodium carbonate (soda ash) in a high-temperature furnace. then dissolved in water to create sodium silicate solutions of various concentrations. Sodium silicate is an important material in many industries due to its economic cost and multiple uses, including: Detergent and Cleaning Products, Adhesives, Cement and Concrete, Textiles, Metallurgy Paints and Coatings. Sodium silicate used as well in water treatment processes to precipitate metals and adjust pH levels. There are many formulations of sodium silicate, depending on the amounts of Na2O and SiO2, but they all share the same property of being a glassy solid that dissolves in water to form an alkaline solution [55-57].

2.2.4.3. Dosage of activators

Sodium silicate solutions typically have a weight ratio of SiO_2 to Na_2O ranging from 2 to 3.75, with values greater than 2.85 indicating a balanced solution (Somna et al., 2011). Furthermore, the more Na_2O/SiO_3 in the alkaline solution, the higher the amount of N-A-S-H gel and the smaller the number of pores; besides, increasing in Na_2O/SiO_3 leads to a decrease in the critical size of the pore [58].

Several investigators have used a commercially available potassium silicate solution containing 15.8 wt% K_2O, 24.2 wt% SiO_2, and 60 wt% H_2O (molar ratio of SiO_2/K_2O

= 2.4), 85% pure potassium hydroxide flakes, and faucet water was used (Zhang et al., 2015) for preparation of AAM.

Phoongernkham et al. (2015b) [59] studied the impact of various molar concentrations of NaOH (6, 10, and 14 M) on the development of compressive strength of assumed mortars. The results showed that the compressive strength increased with increasing molarity. Vasconcelos et al. (2013) [60] investigated the effects of different NaOH concentrations (12, 14, and 16 M) on the strength development of mortars. Still, increasing the NaOH content from 12 M to 14 M after (7, 28 and 56) days increased the compressive strength.

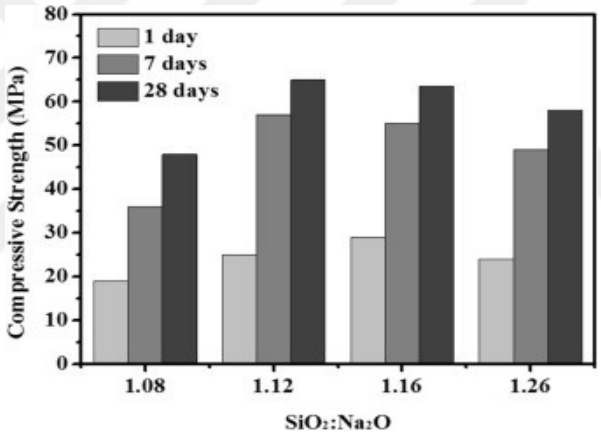

Figure 2.5. Variation ratio of SiO2 to Na2O in the early compressive strength of AAMs" (Hussein et al., 2016) [60].

Hussein et al. (2016, 2018b) [61] investigated the impact of different solution molarities on the development of initial compressive strength of AAM (Fig .25). Mortars with a solution molarity of 14 M (SiO2 to Na2O ratio of 1.16) showed higher initial strength compared to samples with other molarities (10 and 12 M). Fig 2.5 indicates the impact of varying the ratio SiO2/Na2O on the development of compressive strength at early and late ages. (Hussein et al., 2016) reported that increasing the ratio of SiO2 to Na2O (above 2.0) can decrease the strength at ambient temperature.

Zarina Yahya Et. al studied the relation between solid/liquid (S/L) and Na2SiO3/NaOH ratios and the strength of geopolymer paste [62]. They found that when those ratios increased, the compressive strength increases respectively.

As the ratios of (S/L) and (Na2SiO3) to (NaOH) were heightened, there was a simultaneous augmentation in the compressive strength. The highest achieved value of compressive strength materialized when the previous ratios were designated as (1.5 - 2.5) respectively. Moreover, within S/L ratios of 1 and 1.25 until 1.5, the pinnacle value of compressive strength was attained on 2.5 [63].
The compressive strength of the geopolymer paste exhibited improvement with elevated Na2SiO3 concentration. Additionally, the application of Na2SiO3 facilitated an enhanced geopolymerization process by expediting the dissolution of source constituents [64].

An investigation conducted by Hardjito and Rangan [65] unveiled an evident rise in the rate of geopolymerization with escalated Na2SiO3/NaOH ratios. Conversely, surpassing a Na_2SiO_3/NaOH ratio of 3.0 led to a tendency of diminished compressive strength across all S/L ratios.

2.2.5. Curing of Geopolymer

The methods employed to treat geopolymer concrete vary throughout the stabilization and hardening phases. Various treatment approaches impact the mechanical characteristics and overall performance of geopolymer concrete. Furthermore, these methods contribute to the enhancement of strength and durability in geopolymer concrete structures [66]. The geopolymer curing process allows for the examination of how processing conditions effect on geopolymer properties, as well as the impact of different processing techniques on mechanical characteristics such as strength, density, and toughness [67]. When geopolymers undergo a heat treatment process, it accelerates chemical reactions that can impact various mechanical properties, primarily strength, while also resulting in alterations in attributes such as density and toughness [68]. The principles governing the curing of geopolymers encompass a

range of fundamental elements and approaches aimed at achieving optimal development of targeted characteristics [69-70]:

Step 1: Activation of Aluminosilicate Components

Geopolymers typically rely on aluminosilicate constituents, like fly ash or metakaolin. The curing process initiates activation through the stimulation of reactive elements' dissolution, thereby facilitating the creation of geopolymeric gels.

Step 2: Alkaline Setting

Curing takes place within an alkaline environment, often realized by incorporating alkali activators such as sodium hydroxide or potassium hydroxide. This setting triggers the geopolymerization response, leading to the formation of a three-dimensional network structure.

Step 3: Curing Environment

The environment in which curing transpires, whether ambient air or controlled gases, can exert influence over the curing process and eventual properties. Notably, exposure to carbon dioxide can impact the geopolymerization reaction by influencing the alkaline state. Geopolymerization relies on an alkaline medium, typically sodium or potassium hydroxide solutions, which influences the reaction rate and final strength of the product. Air humidity affects water absorption during geopolymer curing. The moisture-to-precursor ratio impacts both geopolymer consistency and reactions, necessitating optimal levels for desired properties. Dry conditions result in water evaporation, which affects hydration and poses a risk of cracks or incomplete curing. While higher temperatures accelerate reactions for faster strength development, excessive heat can lead to issues such as thermal cracks. All these factors collaborate to shape geopolymer performance, including strength, durability, and more. Precise control of the curing environment is essential for achieving the desired material properties during the geopolymerization process.

Samples were subjected to high-temperature heat treatment reaching up to 160 degrees Celsius for durations of 1, 2, and 3 hours. The other type of treatment was conducted under ambient laboratory conditions. Samples of both treatment types were divided into sections, one kept dry and the other humid. After the treatment was completed, all samples were stored in the laboratory until the day of testing. After 2 and 28 days,

geopolymer pastes were used in tests, and the results of treated samples were compared under various conditions.

Procedure 1: Curing Temperature and Duration

The temperature and duration of curing hold a pivotal role in achieving the desired attributes. While heightened temperatures can expedite the geopolymerization process, excessive levels may jeopardize the structural integrity. Ensuring an appropriate curing period is vital for the complete formation of the gel.

Procedure 2: Moisture and Humidity

Successful geopolymer curing necessitates a controlled moisture environment to sustain chemical reactions. Maintaining adequate moisture content and humidity levels is essential to prevent desiccation and ensure a continuous progression of reactions.

Certain geopolymer formulations gain from subsequent curing, which entails subjecting the material to supplementary curing conditions post the initial curing phase. This practice can lead to improved mechanical characteristics and further refinement of the geopolymeric framework.

Specific applications may introduce limitations to curing conditions, encompassing factors like temperature boundaries, moisture availability, or temporal limitations. Mindful consideration of these constraints is pivotal in tailoring the curing process accordingly.

Comprehending and managing these curing principles is of paramount importance in the production of geopolymers boasting desired attributes and performance characteristics, rendering them well-suited for diverse applications within the realm of construction and allied fields.

2.2.6. Advantages and Disadvantages of Geopolymer

Geopolymer cement does not definitely lean on calcium carbonate and it releases approximately 40% to 80-90% less CO_2, during manufacturing, unlike Portland cement which is amongst the most considered one of the most aggressive materials on

the subject of environment [71]. For this reason, geopolymer concrete is considered environmentally friendly concrete in comparison to OPC, and its resistance to chemical acid and fire resistance is superior to OPC concrete resistance, which is a satisfactorily significant indicator for those who positively consider environmental problems as a priority.

The design of geopolymer concrete mixes is more complicated as many parameters are engaged in their development [72]. The behavior and essential qualities of geopolymer concrete are affected by several parameters, e.g. the density of the activators, such as the molarity of NaOH [72], the proportion of silicates to hydroxides [72], silicates modulus [72]; also many factors have a major effect on geopolymer concrete and lead to a more sophisticated mixture designing, like cure time and temperature [73], the activator's pH , water-to-solids ratio , chemical structure and kind of essential material, Si to Al ratio in the geopolymer , mixing and resting time, the Na_2O-to-H_2O molar ratio [73]. To generate geopolymer concrete either the total aggregate content is fixed or coarse and fine aggregate content is fixed purely on the weight ratio basis, in the majority of the methods available or offered, till now, for mixture designing and these methods also did not take in account the specific gravity of raw materials [74-75].

After all, it is still a little risqué for AAMs and GPC to compete with OPC and find a place in the market because of the deficiency of a long track record correlating to indecision in predicting occupational lifetime assumed from investigational durability experiments [76].

2.3. LITERATURE REVIEW

Nowadays most of researches focuses on Alkali-Activated Slag Cement and Concrete (AASCC) to describe the reaction processes, the effect of slag and activator compositions and the development of the microstructure, as well as to attempt to investigate how these factors effect on strength and mechanical properties. z Experiments have proven that slag cement is similar in composition to Portland cement, and they found that partial replacement of cement with cement slag has

advantages that lie in improving the long-term durability of concrete. AASCC is particularly suitable for ready-mix concrete as well as the heat treatment of AASCC has the role of improving mechanical properties at an early age. [77,78]

Usually, the strength of fly ash geopolymer consists of calcium silicate hydrate is slow and heat curing up to 80 ºC is usually employed to help increase the reaction [79].

Hakem Aziz I, et al. (2017) [80] made a study on steel slag and ferronickel slag as raw materials, where they mentioned two types of slag used, the first type was made from iron, such as furnace slag and iron steel slag, and the second type was derived from non-ferrous metals such as lead, nickel and copper slag in addition to using a mixture of sodium silicate solution and sodium hydroxide solution as alkaline activator. where their aim of the study was to shed light on the importance of reducing industrial waste and to study the properties of alkali activated steel slag and the possibility of benefiting from it through experiments. In their paper, they presented information about the results of experiments on compressive strength and compressive properties of metal in addition to the results obtained through the alkaline activation of the slag. In the mineral analysis, they found that the used steel slag contains some rare minerals such as larnite and akerminite. alkali-activated steel slag exhibited low amorphous material, the highest value of strength was obtained after 14 days, The compressive strength of the AAS1 achieved the highest strength at 21.56 MPa, Besides, it setting time of 30 min fully harden and excellent water absorption (3.7 weight%) at 7 days curing. Regarding the porosity, the best value was obtained after 7 days of treatment.

Collins and Sanjayan. (1999) [81] conducted an investigation using granulated blast furnace slag and OPC. Their experimental approach involved the use of different activators and adjuncts, which included powdered and liquid sodium silicate, hydrated lime (L), liquid sodium hydroxide (NaOH), and sodium carbonate (Na_2CO_3). To achieve a consistent chemical composition, NaOH was added to the liquid sodium silicate, aligning it with the dry powdered sodium silicate activator. In order to facilitate a comprehensive comparison, the study adopted the term water/binder (w/b) ratio instead of the conventional w/c ratio. The liquid sodium silicate, NaOH, and a 1% lime-water slurry of hydrated lime were added to the mix along with the mixing

water. Results indicated that at a w/b ratio of 0.5, concrete containing slag activated by powdered sodium silicate exhibited minimal slump loss over a 2-hour period. Conversely, concrete activated with liquid sodium silicate showed significantly reduced initial workability and experienced notable slump loss. Concrete activated using a combination of NaOH+ Na_2CO_3 (H/C) also exhibited substantial slump loss within 2 hours. Comparing one-day strength, activated slag concrete demonstrated similar strength to OPC concrete, while displaying higher strength at later ages. The H/C concrete displayed moderate strength gain beyond three days. Notably, AAS and H/C concrete showcased superior drying shrinkage properties compared to OPC concrete.

Wattanachai and Suwan (2014) [82] made a study on Geopolymer using fly ash and GGBFS with alkaline activators (NaOH and Na_2SiO_3). in addition to use CaO, $Ca(OH)_2$ or OPC as additives. Internal temperatures reaching up to 42 °C on the first day and gradually decreasing to 35°C over the next ten days were observed in a cubic yard sample, even with ambient temperatures of 25 to 30 °C. The highest strength was achieved by fine fly ash geopolymer, followed by medium-fineness fly ash and coarse fly ash. The highest strength of Typical OPC where 30.3 MPa in 28 days and Ambient temperature for cube 150 mm^3. the highest strength of GGBFS where 67.0 MPa in 28 days and Ambient temperature for cube 25 mm^3.

Hassan, Arif and M. Shariq (2019) [83] made a study by using Fly ash and limestone aggregates with NaOH and Na_2SiO_3 solutions as alkaline activators. Two curing conditions were implemented. The first involved heat curing in an oven set at 75 °C for 26 hours, The second condition is ambient temperature curing. For the specimens subjected to heat curing at 75 °C, the compressive strength ranged from (10-31) MPa after 28 days. In contrast, under the ambient curing conditions, the compressive strengths at 7 and 28 days ranged between (4-10) MPa. GPC cured at 75 °C exhibited a 57% increase in compressive strength at 7 days in comparison to specimens cured at ambient temperature. Moreover, the strength of heat-cured specimens at 28 days displayed a remarkable 67% increase when compared to samples cured at room temperature.

Norhasni and Shahrizan. (2019) [84] examined a geopolymer samples using coarse and fine aggregates with fly ash, along with the utilization of sodium silicate (Na_2SiO_3) and sodium hydroxide solution (NaOH) as activators. The specimens cured under ambient temperature conditions then half of the samples were subjected to heat curing at temperatures of 60 °C, 70 °C, 80 °C, and 100 °C for 24 hours in the oven. According to the ambient curing, the specimens displayed a gradual and consistent increase in compressive strength throughout the testing period, culminating in the desired strength by day 28. Geopolymer concrete based on fly ash with a NaOH concentration of 12 M exhibited higher compressive strength under both curing conditions. The specimens cured at 80 °C exhibited a compressive strength value of 32.40 MPa. In contrast, the specimens cured under ambient temperature conditions displayed a lower strength value, approximately 50% weaker. The compressive strength demonstrated an increasing trend up to a temperature of 80 °C, but a subsequent decrease was observed at 100 °C.

Azarsa P. and Gupta R. (2021) [85] investigated the impact of elevated temperature on the compressive strength of GPC (Geopolymer Concrete), comprising a mixture of 50% bottom-ash and 50% fly-ash. Two distinct accelerated curing methods were employed. GPC specimens underwent curing under various temperature conditions: ambient, 30 ° C, 45 ° C, 60 ° C, and 80 ° C, each lasting for 24 hours. Subsequently, all specimens were subjected to an additional 28 days of ambient curing. The compressive strengths subjected to steam curing exhibited a remarkable 3.5x enhancement as the temperature escalated from ambient (~10 °C) to 80 °C. In contrast, dry-cured specimens experienced a more modest increase of approximately 2.3x. In light of these compressive strength findings, the steam curing method at 80 °C was discerned as the optimal curing approach for this study. Where the most robust compressive strength was achieved through heat curing at 80 °C for a duration of 24 hours.

Abdollahnejadet Z. et al. (2018) [86] studied microstructural impact of thermal curing on GPC derived from fly ash. Their findings illuminated that thermal treatment led to a more compact paste structure and fewer fissures, attributed to heightened reaction extent and improved adhesion between the amorphous gel and particles. It is worth

highlighting that an incremental rise in compressive strength is conventionally not anticipated beyond 80 °C thus establishing this threshold as the upper limit for curing temperature in the present investigation.

Yener and Karaaslan. (2020) [87] investigated the effects of diverse curing temperature, involving different combinations of temperatures (ambient, 60 °C, 75 °C, 90 °C, 105 °C) and durations (4h, 8h, 24h, 48h, 96h and 168h), on the performance of geopolymer pastes incorporating both pumice and fly ash. The results highlight that, when subjected to curing temperatures of 60 °C and 75 °C, the compressive strength of specimens exposed to water-drying cycles exhibits a gradual improvement with longer curing periods. Conversely, for higher curing temperatures (90 °C and 105 °C), extending the curing time beyond 24 hours does not provide additional advantages. Notably, the most favorable strength outcomes, following water-drying cycles, are achieved under the specific curing condition of 60 °C/168h, resulting in a maximum strength of 74.4 MPa. However, it is crucial to note that achieving a high compressive strength under dry conditions does not necessarily guarantee the production of a high-quality geopolymer material. Moreover, it's worth mentioning that overly prolonged curing times exceeding 24 hours do not yield favorable results, particularly for elevated curing temperatures such as 90 °C and 105 °C. The optimal duration for achieving peak performance is contingent upon the specific curing temperature employed.

Cengiz Duran ATİŞ et al. (2020) [88] made a study on class F geopolymeric mortar produced by using class F fly ash activated by sodium hydroxide with standard Rilem sand, sodium hydroxide, and water. heat curing was at 75 ºC for 24 hours in addition to ambient curing. After the initial 24-hours heat curing at 75 °C, the geopolymer mortar samples achieved a compressive strength of 32.4 MPa on the first day. Following an additional six months of curing subsequent to the initial 24-hour heat curing at 75 °C, the geopolymer mortar samples exhibited an average compressive strength value of 45.5 MPa. Notably, geopolymer mortar samples cured at ambient temperature reach a compressive strength of 2.1 MPa after 28-days. During extended curing durations of 90 days and 180 days at ambient conditions, the geopolymer mortar samples displayed compressive strengths of 17.2 MPa and 27.1 MPa, respectively.

Bezabih T. et al (2023) [89] This study considers an alternative to high-temperature heat curing of geopolymer mortar using ambient heat curing and a 75 °C in oven. different mixtures of teff straw ash (TSA) and fly ash (FA) in geopolymer mortar mixtures were used. Two curing conditions were performed: ambient temperature and oven curing at 75 °C for 24 hours. After curing, the geopolymer samples were removed from the oven and cooled naturally at room temperature. The compressive, flexural and tensile strengths of geopolymer mortars were evaluated after 7, 14 and 28 days of curing. The results showed that the use of TSA can eliminate the requirement of high temperature geopolymer curing. The compressive strengths cured for 28 days ranged from 45 to 53 MPa at ambient curing temperatures. The highest flexural strength was 9.12 MPa. The inclusion of a higher TSA content enhanced the flexural strength and direct tensile strength of the mortar. For example, where a 10% TSA content led to significant increases of 40%, 59%, and 30% in direct compressive, flexural and tensile strength, respectively, after 28 days.

Shinde B. H., Kadam K. N. (2016) [90] made a study focused on geopolymer mortar development using specific materials included unprocessed fly ash (90% of the mixture), hydrated lime and ordinary Portland cement (OPC), sodium hydroxide and silicates as alkaline activators. Two curing conditions were applied. The first is oven temperature curing temperature 80 °C for 24 hours, preceded by a 1-day rest period. the second is ambient curing condition. In total, 12 different mortar mix compositions were investigated. The mixture containing 12 % OPC with ambient curing showed greater strength than a mixture composed solely of fly ash but subjected to temperature curing. In geopolymer mortars with lime, compressive strength increases to 18 MPa while lime is 8 %. However, when lime beyond 8 %, the compressive strength drops to 14 MPa, specifically for ambient curing conditions. Out of all the groups, the group that contained 20 % OPC exhibited the highest compressive strength, reaching a value of 29.94 MPa.

Moradikhou S. and Moradikhou A. (2021) [91] explored the effects of different combinations of materials and curing conditions on the compressive strength of Geopolymer Concrete (GPC). The materials included Class C fly ash, Class F fly ash, and sand, while the activator solutions comprised four groups with different

compositions: Na_2SiO_3 (SiO_2/Na_2O) + NaOH, Na_2SiO_3 (SiO_2/Na_2O) + KOH, K_2SiO_3 (SiO_2/Na_2O) + NaOH, and K_2SiO_3 (SiO_2/Na_2O) + KOH. The curing conditions employed included ambient temperature and dry curing in an oven at 80 °C and 90 °C for various durations (6, 12, 18, 24, 30, and 36) hours. Results indicated that using sodium hydroxide and sodium silicate in ambient curing conditions resulted in higher compressive strength and lower permeability. Heat curing significantly increased the compressive strength compared to ambient temperature curing, especially in Na-based GPC specimens. When the curing temperature was increased from ambient to 80 °C, a substantial improvement in compressive strength was observed. However, beyond 90 °C, there was no significant further increase in compressive strength. It was observed that specimens cured at ambient temperature achieved 72% and 81% of their 28-day compressive strength in 3 and 7 days, respectively. In contrast, specimens cured at 80 °C achieved 87 % and 92 % of their 28-day compressive strength in the same time frames. Specifically, the compressive strengths achieved under different conditions were as follows: 70.4 MPa at ambient conditions, 94 MPa at 80 °C, and 95 MPa at 90 °C.

Liu J. et al, (2023) [92] made a study on the influence of two different curing conditions on geopolymer mortar: 40 °C in water and 40 °C in oven, over 7 days and 28 days. by using raw materials included ground granulated blast furnace slag (GGBS), fly ash (FA), and alkaline activators. The experimental results revealed that the heat curing condition proved to be the most effective, where the compressive strength under the influence of water curing ranged from 18.3 to 50.3 MPa for 7 days and 28.4 to 58.2 MPa for 28 days. Correspondingly, the flexural strength ranged from 2.5 to 5.9 MPa for 7 days and 3.1 to 6.9 MPa for 28 days. Furthermore, Under the influence of heat curing the compressive strength exhibited a range of 32.2 to 60.3 MPa for 7 days and 48.1 to 76.3 MPa for 28 days, while the flexural strength spanned from 3.2 to 6.6 MPa for 7 days and 4.2 to 7.4 MPa for 28 days. Notably, the highest compressive strengths of 60.3 MPa at 7 days and 76.3 MPa at 28 days. Interestingly, when compared to the initial two curing conditions, the 40 °C heat curing condition exhibited superior strength, showcasing enhanced mechanical properties attributed to the optimal curing temperature.

Poloju k. and Srinivasu k. (2021) [93] conducted an experimental study amid to examine the impact of traditional oven curing methods with outdoor curing for achieving the desired target strength of geopolymer concrete using fly ash and GGBS as binder materials. They used in their mix fly ash, GGBS, fine aggregate and coarse aggregate, sodium silicate, and sodium hydroxide. The study involved casting various specimens with and without GGBS (at levels of 10%, 20%, and 30%) in fly ash, using different strength activator ratios (1.5 and 2.5). Compressive and split tensile strength tests were conducted at 7 and 28 days under both ambient and oven curing conditions at 60 °C for 24 hours. The results indicated a significant increase in compressive strength as GGBS content increased, regardless of the strength ratio and curing method. The optimal strength was achieved with a strength ratio of 1.5 and a 30% GGBS replacement under oven curing. Comparatively, the oven-cured specimens exhibited moderately higher strength than those cured under ambient conditions, attributed to the accelerated polymerization in higher-temperature curing environments. The highest compressive strength achieved was 42 MPa under oven curing.

Nath P. and Sarker P. (2014) [94] studied the effect of fly ash-based geopolymers for efficient curing without high heat. A mix of Class F Fly ash and ground granulated blast furnace slag (GGBFS) was used. The activator solution contained sodium hydroxide (NaOH) and sodium silicate (Na_2SiO_3), while natural sand acted as fine aggregate. Eight geopolymer mixes were created to study effects on workability, setting time, and compressive strength. The first Curing condition is ambient curing (20–23 °C). The second is oven-cured at 60 °C for 24 hours. The results showed that the compressive strength was around 10 MPa for each 10% slag increase after 28 days, where mixtures containing 10%, 20%, and 30% GGBFS of the total binder demonstrated strength increases of 33%, 74%, and 110% respectively, in comparison to the strength of the control geopolymer mixture (with no slag). Furthermore, the compressive strength showed an increase of around 10 MPa for every 10% rise in the slag content after the 28-day period. They observed that by incorporating up to 30% slag, the maximum compressive strength reached 55 MPa for concrete and 63 MPa for geopolymer mortar at 28 days. Besides, progress beyond 56 days post-heat curing was minimal.

Alexander A.E. and Shashikala A.P. (2022) [95] The study focused on utilizing Fly Ash (FA) and Granulated Blast Furnace Slag (GGBS) as key components. Alkaline liquid combined NaOH with Na_2SiO_3. Fine aggregate was also employed. The binder consisted of FA and GGBS in a 1:3 ratio, and superplasticizer was added to maintain a flow value between 75% and 105%. The superplasticizer's content was 2% by weight of the binder, and the water-to-weight ratio was 7% by mass of the binder. Mixing weights were standardized for all blends. Thus, this study examined 10–30% FA replacement with GGBS to determine the optimal proportion. The study explored the mechanical, microstructural, and durability properties of FA-GGBS-based geopolymer mortar cured at ambient temperature. From the results, it was observed that the replacing even 10% of FA with GGBS significantly reduced the setting time of geopolymer paste, eliminating the need for oven curing. This makes it suitable for on-site applications. Compressive strength for geopolymer mortar with 10–30% FA replacement with GGBS ranged from 40 to 60 MPa. the results showed that the optimal blend for geopolymer mortar was F70:G30, using 10 M NaOH, Na_2SiO_3/NaOH ratio of 2, AL/B ratio of 0.5, EW/B ratio of 7%, and 2% superplasticizer. This blend exhibited strength up to 60 MPa under ambient temperature curing, surpassing the 54 MPa compressive strength of OPC control specimens.

Luan Y. et al. (2023) [96] conducted an experimental study amid to enhance strength properties by introducing an additional waste material, flue gas desulfurization gypsum (DG), which can be considered a component of ternary alkali-activated materials (AAMs). The study focuses on alkali activation and the combination of fly ash (FA) and ground granulated blast-furnace slag (GGBS). DG's effects on GGBS-FA AAMs' strength performance were investigated too. For samples preparation, FA, GGBS, and DG were mixed with sodium hydroxide. The alkaline activator was then mixed with the raw materials. Ambient curing was conducted in their study. From the results, it was observed that the strength of AAMs increased rapidly in the first 3 days, stabilizing at 7 days. The 3-day curing achieved approximately 76.92%, 79.70%, and 76.84% of the 14-day curing's final strength. Compressive strength in the S60 group increased from 11.76 MPa without DG to 14.48 MPa with 6% DG, showing a 23.07% increase. However, further increasing DG content to 12% led to a downward trend in strength for both S60 and S70 groups due to increased calcium content.

Rao A and Kumar D. (2023) [97] made a study aimed to examine the production of geopolymer concrete through parametric optimization, as well as analyzing the strength and durability properties of geopolymer concrete. The materials used include fine aggregate, coarse aggregate, Class F fly ash, ground granulated blast furnace slag (GGBS), and alkaline activators (NaOH, Na_2SiO_3). All samples were subjected to ambient curing at room temperature. The higher calcium content in the GPC grade being studied contributes to the development of a dense structure and improved impermeability. The analysis of atomic elements confirms the presence of C-S-H and N-A-S-H, distinguishable by their unique form, shape, or structure. The water absorption rate for 14 M GPC is 2.865%. The maximum compressive strength was achieved after 28 days 52 MPa for samples immersed in Na_2SO_4 and $MgSO_4$ then started to decrease after 56 days where it reached a value 49 MPa and 47 MPa for 90 days.

Chouksey A. et al. (2022) [98] The main goal of this study was to explore the impact of different curing conditions on specimen properties: physical, mechanical, and microstructural. The investigation encompassed both ambient and oven curing methods. The materials used were fly ash, GGBFS binders, coarse aggregates, M-sand as fine aggregate, and alkaline solutions with sodium hydroxide and sodium silicate. Two curing techniques were employed: ambient and oven curing at 80 °C for 24 hours. Ambient-cured specimens demonstrated higher density, Poisson's ratio, and dry shrinkage compared to oven-cured counterparts, indicating superior quality and strength in the latter. Oven-cured specimens also displayed higher flexural strength. The maximum splitting tensile strength was 4 MPa for ambient-cured and 5.2 MPa for oven-cured specimens after 56 days. Both ambient and oven-cured specimens retained 98% of their flexural strength. In a 28-day test, ambient-cured GPC specimens showed a flexural strength of 3.8 MPa, while oven-cured GPC specimens exhibited higher flexural strength at 5.5 MPa.

Mehmood A.B. et al. (2019) [99] made a study aimed to investigate the benefits of incorporating foundry sand into heat-cured fly ash-based geopolymer concrete. Geopolymer mortar specimens underwent both ambient curing and oven curing, spanning a temperature range of 60 °C to 90 °C. The results indicated that heat-cured

geopolymer concrete achieved 95% strength at 7 days and reached 100% at 28 days. Under ambient conditions, the strength ranged from 60% to 70% at 7 days. The results showed that the addition of 10% foundry sand replacement led to a strength improvement of 10-25%. Heat curing significantly increased strength by up to 70%. The highest strength was achieved through heat curing at 90 °C for a duration of 24 hours, measuring 54 MPa after 28 days. Regarding tensile strength, replacing 10%-20% of foundry sand during heat curing enhanced the strength by 30% at 28 days, resulting in the highest value of 6 N/mm². In conclusion, heat curing demonstrated markedly superior strength compared to ambient curing.

PART 3

MATERIALS AND METHODS

3.1. MATERIALS

In this study, geopolymer mortars and pastes were formulated based on Ground Blast Furnace Slag (GBFS) and Ground Granulated Blast Furnace Slag (GGBFS) as precursors from KARABÜK KARDEMIR Iron and Steel Factory as byproducts of steel production. In addition to these, steel slag, Energy Terminal System Ash, and MEROS Ash were integrated to enhance physical and mechanical properties of the geopolymer materials. Sodium hydroxide in pellets form and sodium silicate in aqueous form were used to obtained geopolymer structures in the materials. Detailed properties of the and information are given below.

3.1.1. Granulated Blast Furnace Slag (GBFS)

In this study, GBFS were collected from KARDEMIR Karabük Iron and Steel Factory from the plant. It is manufactured by introducing molten slag into the granulation tank at approximately 1500 ° C. Molten slag is blasted with a cold-water spray. GBFS is pumped to the dewatering drum. The dewatering drum separates the granulate from the water and the granulate is precipitated fed on to the conveyor. GBFS produces a fine 0/4 mm, shown in Figure 3.1a, glassy aggregate used for multiple construction applications, primarily its use is as a cement replacement when ground to a fine powder. GBFS is coarse, amorphous and sand-sized material. The average of its particle size ranges from 1 to 1.5 mm [100]. Physical and chemical properties of the GBFS are given in Table 3.1 and 3.2. respectively.

3.1.2. Ground granulated blast furnace slag (GGBFS)

GGBFS used in this study conformed to ASTM C989 is processed by drying and ground using a horizontal ball mill into a fine powder nearly pristine white appearance as shown in Figure 3.1b, derived from KARÇIMSA Cement Factory in Karabük. Physical and chemical properties of the GGBFS are given in Table 3.1 and 3.2 respectively. Microstructure images and mineralogical analyses are presented in Figures 3.2 and 3.3 for GGBFS and EPA, correspondingly.

Figure3.1. a) GBFS, b) GGBFS.

Table3.1. The physical properties of all solid components.

Components	Unit	GBFS	GGBFS	EPA	SS
Bulk density	(kg/m^3)	1240	1200		1400
Specific gravity	(g/cm^3)	0.65 – 1.10	2.9		2.8
Specific surface	(m^2/kg)	300 - 600	425 – 470		500
Color		Brown granules	White powder		Gray
Residue 100 µ	%	51.21	-		
Passing 100 µ	%	41.90	100		
Passing 45 µ	%	-	70		33.15

Table3.2. The chemical properties of components.

Components	Unit	EPA	GBFS	GGBFS	SS
SiO_2	%	50.74	35.0 – 45.0	40.4	14.73
Al_2O_3	%	28.01	9.0 – 13.0	10.6	2.44
Fe_2O_3	%	7.998	0.1 – 3.5	1.28	19.53
MnO	%	-	-	-	4.15
CaO	%	5.435	30.0 – 40.0	34.19	44.88
MgO	%	2.114	6.0 – 8.5	7.63	12.65
S	%	-	-	-	0.14
P_2O_5	%	-	-	-	0.97
K_2O	%	1.120	0.5 – 2.0	1.120	0.01
TiO_2	%	1.312	0.3 – 0.7		0.48
Na_2O	%	1.364	0.2 – 0.6	1.364	0.01
Baz	%	0.100	-	-	3.351
Loss of ignition	%	2.07	-	2.74	-
SO_3	%	0.768	-	-	-

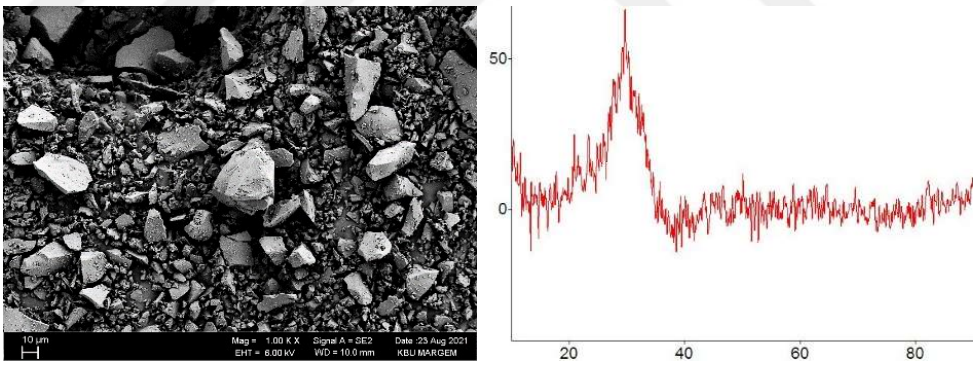

Figure3.2. SEM image and XRD pattern of GGBFS [101].

Based on Figure 3.2, GGBFS particles exhibit sharp and indeterminate geometric configurations, and the majority of the observed GGBFS particles are smaller than 45 microns. Based on the XRD pattern, GGBFS exhibits an amorphous structure with increased calcite, quartz, and alumina peaks. Figure 3.3 displays an SEM image of EPA, which reveals two distinct regions. These areas exhibit a large number of small spheres ranging from nanometer-sized to micrometer-sized and occasional sharp structures. The XRD pattern of EPA indicated a high silica content with low calcium

and aluminum peaks. Furthermore, the mineral structure includes quartz, calcite, tridymite, and clay.

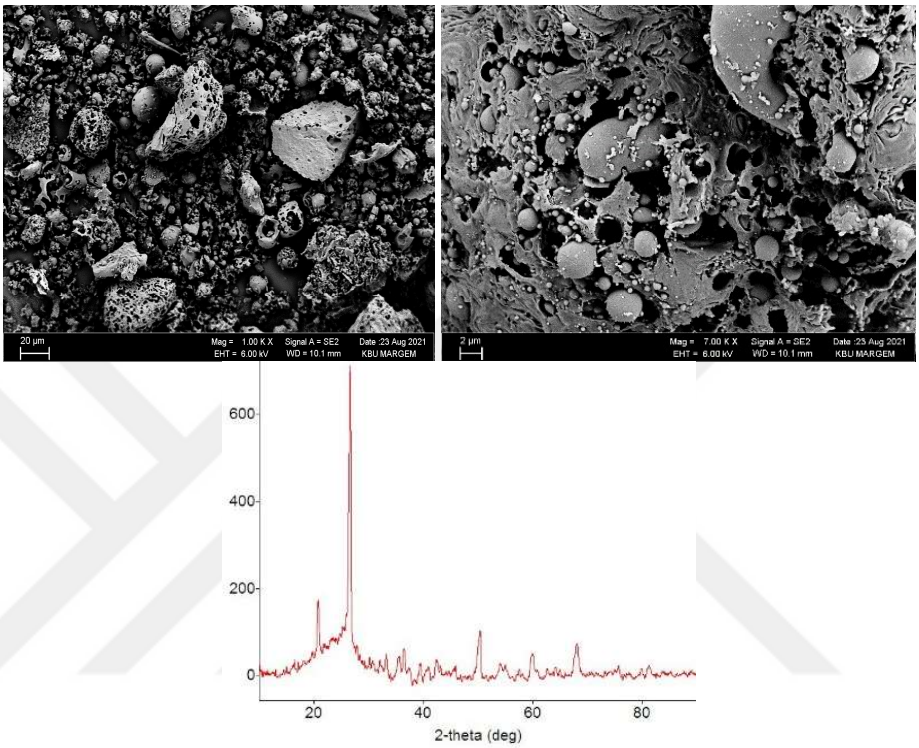

Figure3.3 SEM images and XRD pattern of EPA [101].

3.1.3. Steel Slag

Steel Slag (SS) shown in Figure 3.2a-b is collected from KARDEMIR Iron&Steel factory in Karabük. Figure 3.2a shows SS above the 2 mm sized sieve, Figure 3.2b shows SS after the sieving process. The physical and chemical properties of SS are given in Table 3.1 and 3.2, respectively. according to Table 3.2, SS includes Fe_2O_3, CaO, Al_2O_3, MgO and SiO_2 substances as the main components depend on the process in which they are manufactured.

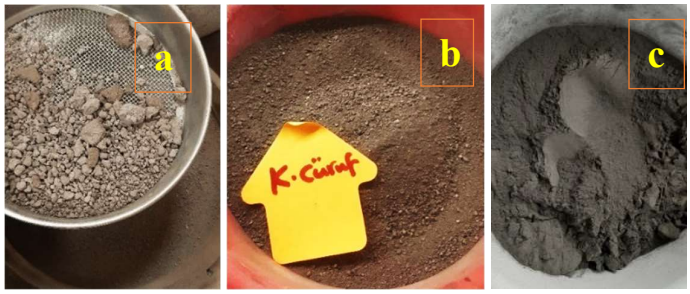

Figure3.4. a) SS above the 2 mm sized sieve, b) SS after the sieving process, c) EPA

3.1.4. Energy Terminal System Ash (EPA)

Energy terminal system ash (EPA) as shown in Figure 3.2c is similar to the Fly ash composition, like low calcium fly ash (Type F). The physical and chemical properties of SS are given in Table 3.1 and 3.2, respectively. according to Table 3.2, the high loss on ignition ratio notifies negatively affects the water demand and reactivity index. SEM and XRD analysis of the EPA are shown in Figure 3.5.

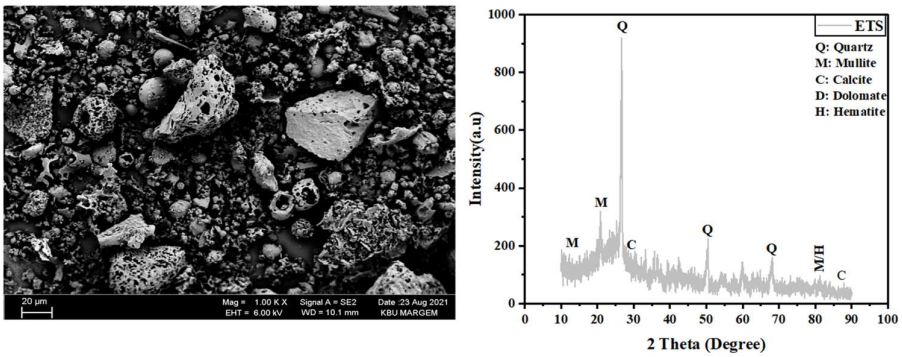

Figure3.5. SEM images and XRD pattern of EPA [101].

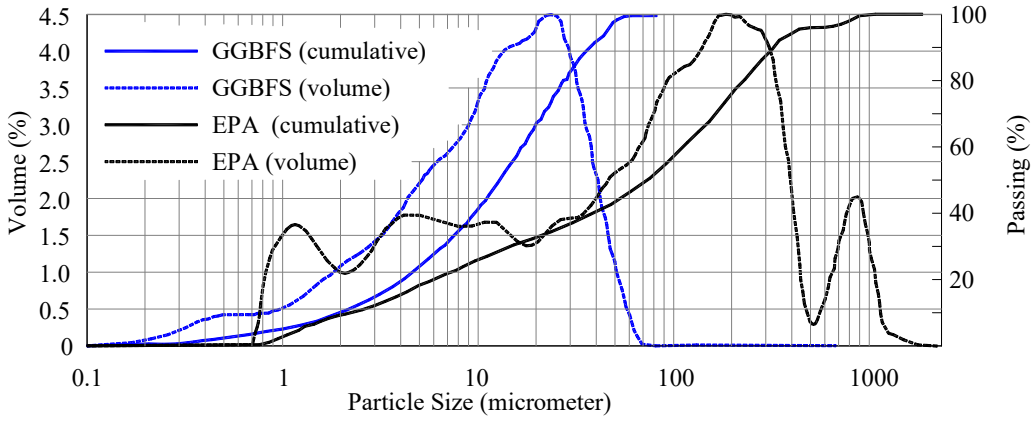

Figure3.6. Particle size analysis of GGBFS and EPA [101].

The results of particle size analyses for both GGBFS and EPA can be seen in Figure 3.4. These analyses reveal that the D90, D50 and D10 values of GGBFS are 38.7 µm, 13.85 µm, and 1.9 µm, respectively, and for EPA, the values are 123.8 µm, 75.6 µm, and 12.4 µm, respectively. As a result, the analyses demonstrate that the particle size of EPA is coarser than that of GGBFS. Based on Table 2, the pozzolanic activity index for the EPA was higher than that of GGBFS at an early stage of 7 days, despite the fact that the particle size distribution of the EPA is coarser.

Furthermore, the particle volume distribution of EPA is more dispersed than GGBFS. Unlike Fly Ash, there is little control over the collection of EPA in the Energy Production System, while GGBFS is ground before use. Approximately 16,000 tons of EPA are produced annually by KARDEMIR Iron&Steel Factory. While this component exhibits a lower reactivity index on the 28th day and a higher heating loss and water requirement than GGBFS, hindering its extensive usage.

3.1.5. MEROS Ash (Sinter Ash)

MEROS ash is created as a result of operation at the Maximized Emission Reduction of Sintering (MEROS) facilities of the KARDEMIR Iron and Steel factory, produced from iron-containing flue dust formed during the process in a sintering facility. It is a dry type of gas cleaning technology to reduce harmful emissions from sinter plants. The amount of MEROS processing waste is about 90,000 tons/year (2023). In

experimental studies, MEROS ash as shown in Figure 3.3 is utilized either as a compound or in terms of its contributing to the activators by being dissolved. During initial tests, MEROS ash was successfully dissolved in water and Na_2SiO_3 at room temperature. MEROS ash has several impurities such as Zn, Cu, As, Pb, Mn, Fe as shown in Table 3.3.

Figure3.7. Meros Ash

Table3. 3 Semi-Quantitative Phase Analysis Results with XRD (mg/kg).

Na	Mg	Al	K	Ca	Mn	Fe	Cu	Zn	As	Pb
440.5	260.8	473.1	6.05	1.11	156.3	7.24	464.4	318.4	212.7	1.26

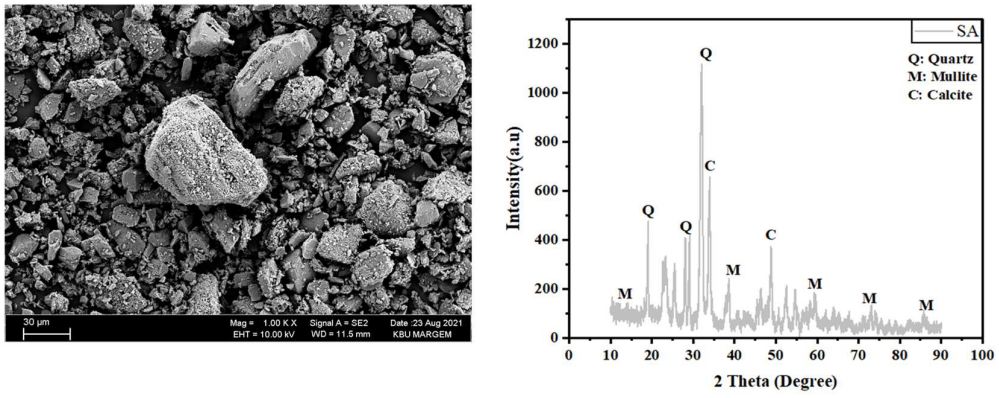

Figure3.8. XRD analysis and SEM images of SA [101]

Table3.4. Metal Analysis Results.

Analysis	Results (%)	Method	Analysis	Results (%)
Na_2SO_4	85.90	TS 4528:1985	CaO	2
Na_2CO_3	1.50	ISO 6353/2:1983	SO_3	45.63
NaCl	7.20	ISO 6353/2:1983	Free lime	4
NaF	1.00	Ion Chromatography	LOI	4.5
PH value	8	ISO 6353/2:1983	Na_2O	20
Fe_2O_3	6		K_2O	1

3.1.6. Alkaline Activators

Na_2SiO_3 in aqueous form and NaOH in pellet form were used as alkaline activators to prepare geopolymer materials. Sodium silicate in aqueous solution is commonly called "liquid glass" or water glass [102]. Its important characteristic is its solubility in water, and in fact sodium silicate is marketed mainly in liquid form. Because of this distinctive property of solubility and the glassy nature of the solid. Is an inorganic sodium salt having silicate as the counterion. It contains a silicate ion. The commercial product, available in water solution or in solid form, is often greenish or blue owing to the presence of iron containing impurities.

The chemical and physical properties of Na_2SiO_3 are given in the Table 3.5. A sodium silicate solution (Na_2SiO_3) with 10 M sodium hydroxide (NaOH) in different proportions and mixed as an alkaline activated solution was used in order to activate the ashes of EPA and GGBFS as shown in Figure 3.4.

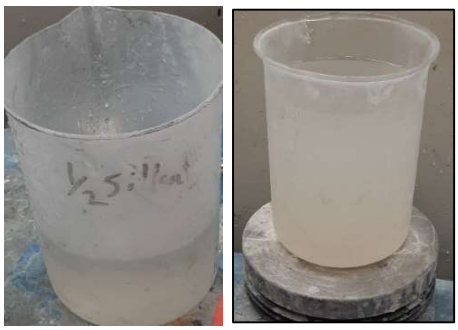

Figure3.9. Sodium Silicate (Na2SiO3) and 10 M of NaOH liquid

Table3.5. The chemical and physical properties of Na_2SiO_3 [102].

Property	Amount
Density (g / cm^3)	1.396 – 1.418
Na_2O (wt %)	11.3 – 12.9
SiO_2 (wt %)	22.6 – 25.8
Module (SiO_2/ Na_2O)	1/2
pH	11-13
Refractive Index	1.40 -1.46
Appearance	colourless

The Sodium Hydroxide (NaOH) is commonly called as caustic soda and it is available in flakes or pellets form with 97%-98% purity [103]. It is a white solid compound. NaOH can react with moisture from the air and may generate heat as it dissolves, also dissolves in water easily and reacts with dilute acids to form sodium salt, acid, and water. According to the requirement concentration the NaOH solids were dissolved in water to make the solution. In the process of polymerization, the most common alkali-activated solutions to start the activation of reactions are a mixture of NaOH and Na_2SiO_3. To prepare 10 M of NaOH liquid, the NaOH pellets were dissolved in distilled water (400 g NaOH and water in 1 liter volume) as shown in Figure 3.4.

3.2. EXPERIMENTAL METHODS

3.2.1. Preparing of Geopolymer Pastes

Two different groups of mixtures were produced in this study; in the Group 1: GBFS were used as a precursor with EPA, in the Group 2: GGBFS were used as a precursor with EPA to produce geopolymer pastes. In addition to these, MEROS ash were used to improve activator effects in all geopolymer pastes. The mix designs of the geopolymer pastes are given in Table 3.6. In order to prepare the geopolymer materials, initially, the activator solution as 50% Na_2SiO_3 + 50% 10 M NaOH was mixed with the MEROS ash as 5% by weight of Na_2SiO_3+NaOH. They were mixed until a homogeneous solution was obtained. Then, in the mixer container, EPA GGBFS or GBFS and Steel slag were added to the activator solution subsequently and mixed in the mixer for totally 7 minutes.

When the time end, the mixture was poured into the steel molds sized 50x50x50 mm in cubic shapes. Afterwards, the geopolymer specimens were cured at 22±2 ºC, 60 ºC, 80 º C, 120 ºC, 140 ºC and 160 °C for 1, 2, and 3 hours in an oven and then placed to the laboratory at ambient and moisture curing conditions until the test days.

Table3.6. Mix design of geopolymer materials (by weight).

Code	GBFS	GGBFS	EPA	SS	NaOH (10M) (N)	Na_2SiO_3 (NS)	SA/(NS+N)	S/P ratio	Bulk Density
A	-	0.3	0.1	0.3	0.15	0.15	0.05	0.43	2.09
B	0.3	-	0.1	0.3	0.15	0.15	0.05	0.43	2.09

3.2.2. Curing Process

The curing process was conducted in two steps for heat processing: 1) Ambient laboratory condition for 28 days in two categories I. moisture and II. dry conditions, 2) Oven curing at 60 ºC, 80 ºC, 120 ºC, 140 ºC, and 160 °C temperatures for 1 h, 2 h and 3 h to achieve high early strength and then the geopolymer specimens were put into the laboratory conditions in two categories I. moisture and II. dry conditions. Moisture curing was applied to the specimens by placing wet towels over the geopolymer materials. The experimental program is shown in Table 3.7 as well as Figure 3.10.

For high early compressive strength, heat treatment at high temperatures is recommended by Özen (2021) [104]. Samples removed from the oven were kept in cardboard boxes to control shock-free cooling and to protect them from external influences. As for the wet samples, they were covered with a wet cloth to ensure that the wet conditions were achieved.

Table3.7. Study design of Material-based GPs specimens.

Material-based GPs	Curing regimes	Curing Temperature (° C)	Curing time	After heat curing lab. dry condition (Ambient)	After heat curing lab. condition (Wet)
GBFS - based GPs	Ambient	22±2	28 days	G_A	G_W
	Oven curing	60	1 hour	G6_1a	G6_1w
			2 hours	G6_2a	G6_2w
			3 hours	G6_3a	G6_3w
		80	1 hour	G8_1a	G8_1w
			2 hours	G8_2a	G8_2w
			3 hours	G8_3a	G8_3w
		120	1 hour	G12_1a	G12_1w
			2 hours	G12_2a	G12_2w
			3 hours	G12_3a	G12_3w
		140	1 hour	G14_1a	G14_1w
			2 hours	G14_2a	G14_2w
			3 hours	G14_3a	G14_3w
		160	1 hour	G16_1a	G16_1w
			2 hours	G16_2a	G16_2w
			3 hours	G16_3a	G16_3w
GGBFS - based GPs	Ambient	22±2	28 days	GG_A	GG_W
	Oven curing	60	1 hour	GG6_1a	GG8_1w
			2 hours	GG6_2a	GG8_2w
			3 hours	GG6_3a	GG8_3w
		80	1 hour	GG8_1a	GG12_1w
			2 hours	GG8_2a	GG12_2w
			3 hours	GG8_3a	GG12_3w
		120	1 hour	GG12_1a	GG14_1w
			2 hours	GG12_2a	GG14_2w
			3 hours	GG12_3a	GG14_3w
		140	1 hour	GG14_1a	GG16_1w
			2 hours	GG14_2a	GG16_2w
			3 hours	GG14_3a	GG16_3w
		160	1 hour	GG16_1a	GG6_1w
			2 hours	GG16_2a	GG6_2w
			3 hours	GG16_3a	GG6_3w

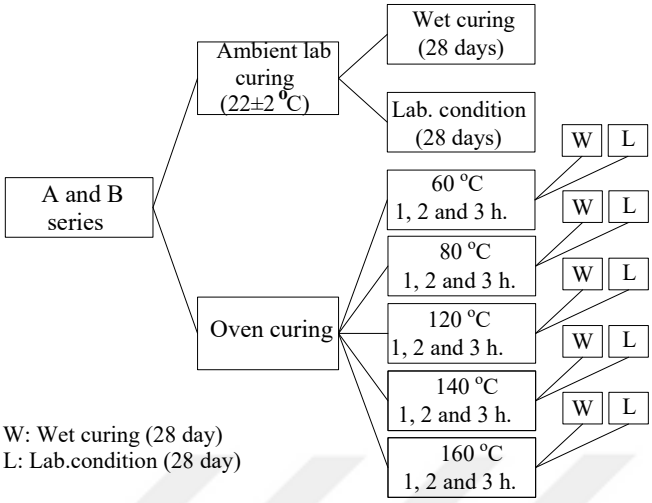

Figure3.10. The scheme of the experiments

3.2.3. Experimental Studies

In the study, the compressive strength test and water absorption tests were conducted on the 2nd and 28th days according to ASTM C109 [105]. After the compressive strength tests at 28th days, X-ray diffraction (XRD) analysis and scanning electron microscopy (SEM) with EDS analyses were performed from the geopolymer materials.

3.2.3.1. The Flow Table Test On Fresh State Geopolymer Materials

Workability was measured by using a flow table test according to ASTM C230/C230M-20 [106]. Flow table equipment was used consisting of a conical mold with dimensions of top diameter 70 mm, bottom diameter 100 mm and mold height 50 mm. At first the flow table was cleaned and dried, then the conical mold was placed and centered on the flow table and all the paste was put into the conical mold as shown in Fig 3.5a. After that, the mold is lifted to flow the mixture and 25 strokes are applied within 25 s on the table by hand of the machine as shown in Fig 3.5b. Then, the flowed geopolymer material diameter was measured from cross lined with a tape measure.

a)  b) 

Figure3.11. Spreading table and spreading diameter measurement.

3.2.3.2. The Compressive Strength Test On Hardened State Geopolymer Materials

The compressive strength test was performed on 50x50x50 mm sized GP specimens according to ASTM C109/109M-16a [105]. Where in the early stages the specimens were weighed to calculate the unit weight (UW), then the test was conducted for all specimens. The compressive strength test machine is shown in Figure 3.6. Where all tests were carried out on the specimens on the 2^{nd} and 28^{th} days. The compressive strength tests results are evaluated from the equation 3.1.

$\boldsymbol{\sigma} = P/A$ (Eq. 3.1)

σ = Compressive strength of concrete (MPa)

P = The used fraction load and its unit (kg)

A = The area or surface area of a concrete cube or a cylinder and its unit (cm^2).

a)  b) 

Figure3.12. Compressive strength test machine

3.2.3.3. The Water Absorption Test On Hardened State Geopolymer Materials

The water absorption test was performed on the geopolymer materials at the 28th days. water absorption test was carried out as described in ASTM C20 [106]. The water absorption test equipment in the experiment mainly consists of weighing and drying oven. Initially, specimens taken from the processing conditions were immersed in tap water for 24 h. as shown in Fig. 3.12b. After 24 h, specimens were removed from the immersion and then dry the surface by placing the specimens in a towel to measure the weight of the saturated dry specimens (M1), as shown in Fig. 3.12a, and then they are weighed in water to measure their weight inside the water (M2) as shown in Fig. 3.12d. Finally, the specimens are kept in the oven at 100 ± 5 °C for 24 h to be completely dried and their dry weight (M0) calculated as shown in Fig. 3.12c. The dry density, water absorption and apparent porosity of the specimens were calculated according to the Eq. 3.2-3.4.

$$W\ (\%) = \frac{M1-M0}{M0} \text{ x } 100 \tag{3.2}$$

$$\delta = \frac{M0}{M0-M2} \tag{3.3}$$

$$Pg = \frac{W*M0}{M1-M2} \tag{3.4}$$

Where; W = Water absorption rate. Pg = Apparent porosity.

δ = Specific gravity. M_0 = Dry weight.

M_1 = Specimen weight in saturated surface dry condition.

M_2 = Specimen weight in water.

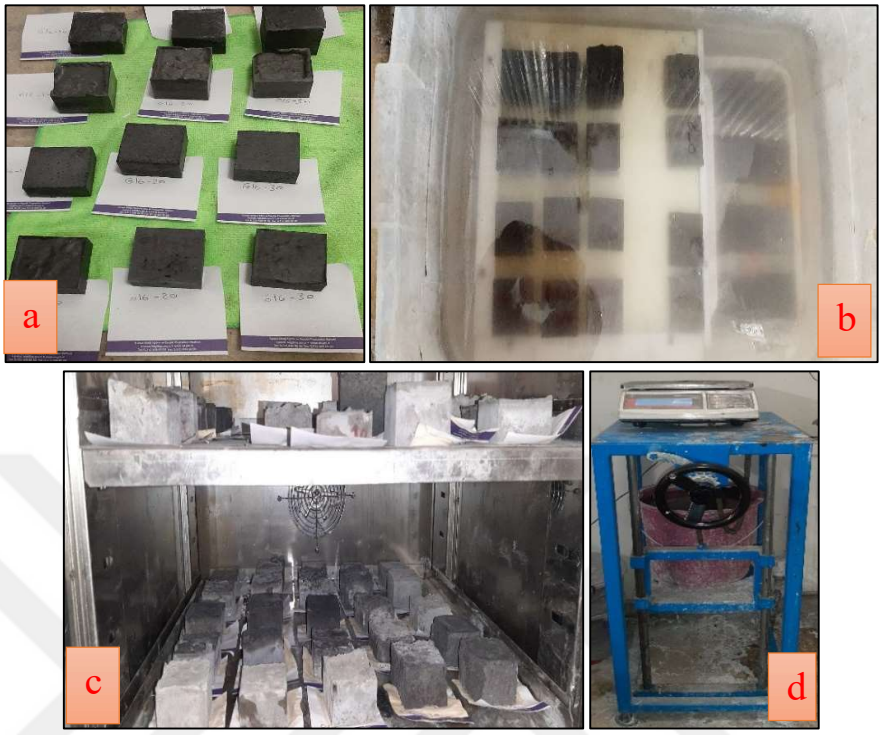

Figure3.13. Representation of water absorption test steps

PART 4

RESULTS AND DISCUSSION

This section includes the results of fresh and hardened geopolymer pastes (GP) and mortars tests as well as discussions on these properties. This section is arranged as the following topics:

- Flow table tests results and discussion
- Compressive strength tests results and discussion
- Unit weight
- Determination of time and temperature difference results
- Effect of humidity
- Water absorption, specific gravity, apparent porosity results and
- Discussion
- Contraction of results and discussion

4.1. FLOW TABLE TEST RESULTS AND DISCUSSIONS

The flow table test revealed that the fresh GBFS-based geopolymer mortars was 17 cm and the GGBFS-based GP was 13.5 cm. As per the results, it was observed that the GBFS-based GPC was more workable than the GGBFS-based GPs.

Figure 4.1. flow table test procedure

4.2. THE UNIT WEIGHTS RESULTS AND DISCUSSIONS

The unit weights (UW) calculated derived from the measurement of weights of the compressive strength test specimens of GBFS and GGBFS-based GPs are shown in Figure 4.1 and Figure 4.2 respectively.

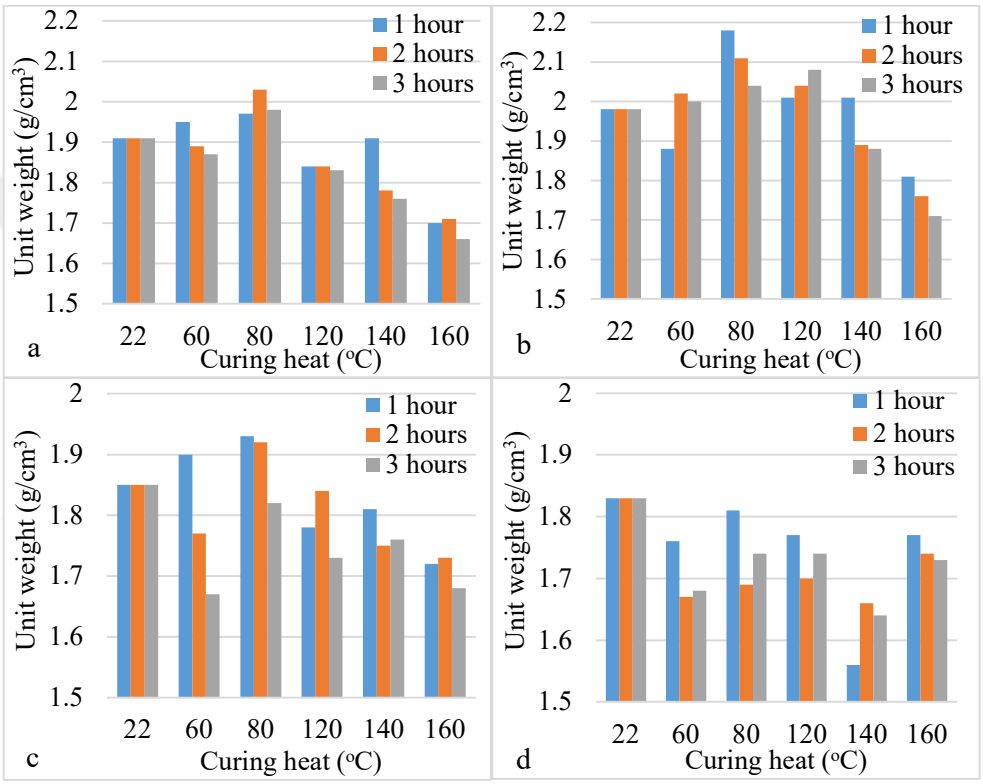

Figure 4.2. Unit weights of the GBFS-based GPs for a) ambient at 2nd day, b) wet curing at 2nd day, c) ambient at 28th day and d) wet curing at 28th day

According to the Figure 4.2,

- According to the results, the UWs ranged between 1.66 – 2.18 g/cm^3 and 1.56 - 1.92 g/cm^3 for the 2nd and 28th days curing periods respectively. The results described can be influenced by several factors related to curing conditions, specific material, physical and chemical properties of the samples.
- The UWs for both wet and ambient curing increase as the curing temperature increases to 80 °C whereas the UWs decrease at higher temperatures than 80 °C for 2nd day measurements. Dry curing involves reducing moisture levels, and the

material's thermal behavior determines UW variations with temperature changes. Higher temperatures may cause void creation, affect the existing pore structure, or volume changes leading to UW changes [107].

- The highest UW (2.18 g/cm³) observed at 80 °C for one hour of curing for all curing periods. In contrast, at 160 ° C, thermal contraction may have occurred, resulting in a reduced UW of 1.7 g/cm³.
- According to the UW measurements of GBFS-based GP for both wet and ambient curing at 28th day, conversely, at 60 ° C with long curing duration of 3 h, leading to a lower unit weight of 1.6 g/cm^3 due to the material thermal contraction or other structural changes.
- Longer curing times does not impact the UW values significantly.

Short curing time at a high temperature might not allow the material to fully densify, potentially resulting in a lower UW. In wet curing conditions, the longer curing duration at 160 °C might have contributed to increased shrink and a higher unit weight of 1.7 g/cm³. Where main materials may expand or contract under specific temperature conditions, affecting their overall density [108].

According to the Figure 4.3,

- The minimum UW were calculated in ambient condition at 160 °C, for 3 hours on 2nd days.
- GP produced with GGBFS has shown an increase in UW, reaching 2.04 g/cm^3, during ambient curing at 80 °C for 2 to 3 hours on the 2nd day. However, the UW gradually decreases until it reaches 1.7 g/cm^3 at 160 °C. During wet curing, the lowest UWs value was 1.5 g/cm^3 when cured at 120 °C for 2 hours.
- The UWs for curing under ambient and wet conditions ranged from (1.8 - 2 g/cm^3) during the 28-days curing period.
- UWs for ambient curing increase with curing temperature up to 80 °C and 120 °C until 2 hours, whereas UWs decrease at higher temperatures than 140 °C for 28-days measurements.
- The highest UWs (2.09 g/cm³) were observed at 60 °C for one hour of wet during the 2-days curing period.

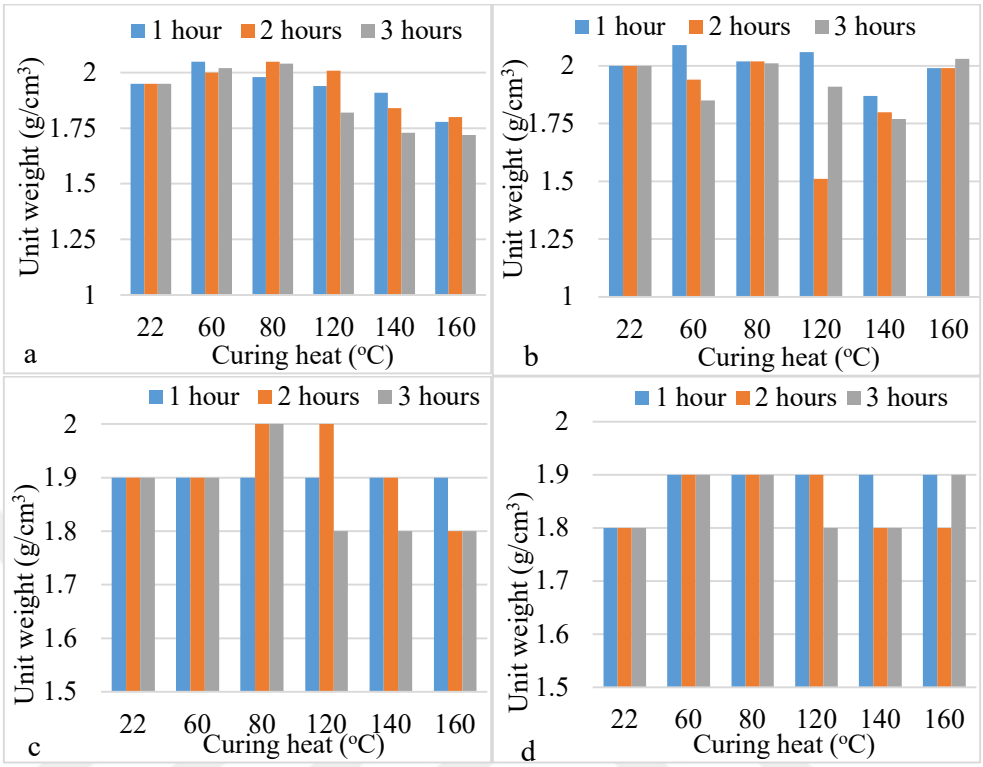

Figure 4.3. UW of GGBFS-based GPs for a) Ambient, b) Wet curing conditions at 2nd day. c) Ambient, d) Wet curing conditions at 28th day.

Geopolymers can exhibit different behavior at various temperatures. The decrease in UW at 160 °C might be indicative of changes in material stability or even degradation under high-temperature conditions [109].

The UW values of the treated samples in both wet and dry conditions after furnace heat treatment showed relatively similar results, particularly at 60 ° C and 22 ° C, where the material may exhibit similar behaviors, resulting in comparable UW values. However, as the temperature increases leading to a decrease in unit weight up to 1.8 g/cm³. Nevertheless, as the temperature increased during dry curing conditions, there was a slight decrease in the UW value, dropping from 2 g/cm³ to 1.8 g/cm³. The difference between wet and dry curing conditions is the moisture content.

4.3. THE COMPRESSIVE STRENGTH TEST RESULTS AND DISCUSSIONS

The compressive strength tests results of the GBFS-based GPs for 2nd and 28th days are given in Table 4.1 and comparisons between the groups are shown in Figure 4.4.

Table 4.1. Compressive Strength and unit weights of GBFS geopolymer paste.

Codes	Compressive strength (MPa)		Codes	Compressive strength (MPa)	
	2 days	28 days		2 days	28 days
G_a	0	13.30	G_w	0	8.50
G6_1a	0	3.60	G6_1w	0	0
G6_2a	0	0	G6_2w	0	0.40
G6_3a	0	2.80	G6_3w	0	0.50
G8_1a	0	4.20	G8_1w	0	2.80
G8_2a	0	2.10	G8_2w	0	2.00
G8_3a	0	2.00	G8_3w	0	2.10
G12_1a	0	2.10	G12_1w	0	0
G12_2a	0	2.40	G12_2w	0	0
G12_3a	0	2.60	G12_3w	0	0
G14_1a	0	2.50	G14_1w	0	0
G14_2a	0	2.70	G14_2w	0	0
G14_3a	2.5	3.70	G14_3w	0	0
G16_1a	3.1	4.00	G16_1w	0	2.60
G16_2a	3.6	3.80	G16_2w	0	3.30
G16_3a	2.5	3.90	G16_3w	0	3.70

According to Table 4.1,

- Most of the compressive strengths at 2nd day period of the GBFS-based GPs are obtained zero due to the lack of geopolymerization reactions between coarse size of GBFS and EPA. Absence of compressive strength may have occurred due to the excessive water content within the paste, compromising its structural integrity.
- The compressive strengths are obtained by curing the GBFS-based GPs for 2 days at ambient conditions after subjecting them to a temperature of 140 ^{o}C

for 3 hours. However, the strengths are weak (<4 MPa). Therefore, the ambient curing regime is more efficient for GBFS-based GPs.

- The compressive strengths at 28th day of GBFS-based GPs are higher in ambient conditions than in wet conditions. Additionally, the majority of GPs have not demonstrated strength in wet conditions.
- The higher compressive strength is observed in ambient curing for 28 days as 13.3 MPa.

Inadequate curing procedures, particularly in wet conditions, can impede the completion of essential chemical reactions that contribute to the development of specimen strength. Because of its granular texture, the specimens did not adhere well and exhibited weak cohesion, especially in the case of wet specimens, where moisture exacerbated their dissociation [110].

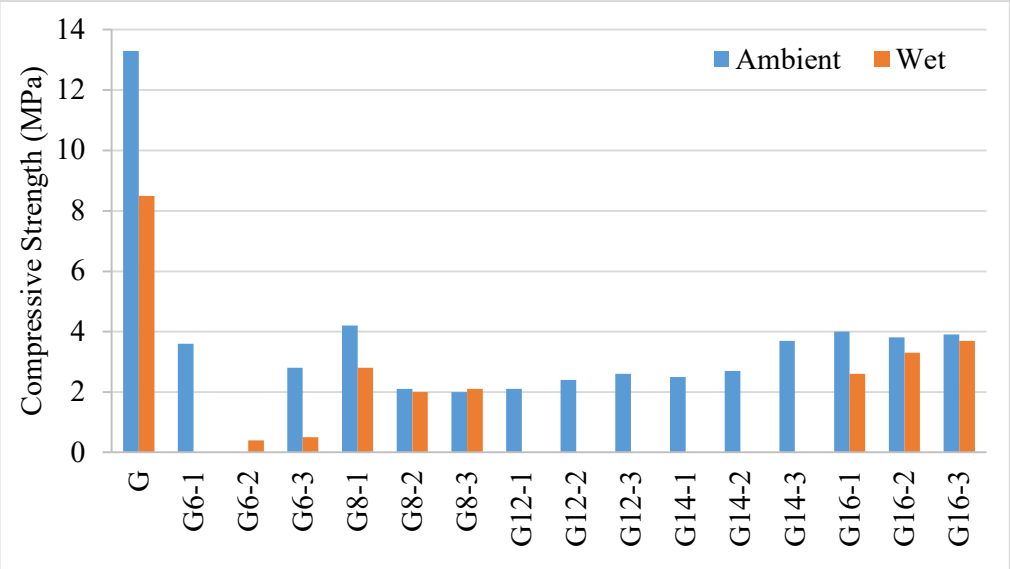

Figure 4.4. Compressive Strength (MPa) values of GBFS-based GPs at 28th day.

According to Figure 4.4,

- The pressure began to increase at 140 °C in dry samples and reached a maximum value of 3.6 MPa when the samples were cured for two hours at 160 °C.

- In the GBFS group, when a temperature of 160 °C was reached for wet and specimens, the compressive strength began to increase.

Geopolymer materials exhibit a heightened sensitivity to elevated temperatures. When exposed to high curing temperatures, excessive heat can induce the thermal degradation of the geopolymer gel [111]. This degradation inhibits the formation of a robust and cohesive geopolymer structure, resulting in an extremely low or zero compressive strength [112]. Moreover, if the curing temperature surpasses the optimal range or if the concrete undergoes rapid and extreme temperature fluctuations, this can lead to overheating [113]. This overheating can cause the geopolymer matrix to destabilize and ultimately prevent the development of compressive strength [114].

The minimum compressive strength achieved was zero. This result is attributed to the geopolymerization process that solidifies geopolymer concrete, requiring an adequate amount of time to develop. The compressive strength value of GGBFS-based GPC under wet curing conditions without an oven for two days is zero. As such, a two-day wet curing period is inadequate for the geopolymerization reaction to occur sufficiently for measurable compressive strength levels to manifest [115].
The compressive strength tests results of the GGBFS-based GPs for 2^{nd} and 28^{th} days are given in Table 4.2 and comparisons between the groups are shown in Figures 4.5 and 4.6.

At 160 ° C the compressive value appeared after 28 days for the wet specimens, while it remained equal to zero at 2 days.

In the GGBFS group, the compressive strength increased at 28 days, especially at temperatures of 80 and 120 degrees. In some cases, new specimens were manufactured, and the experiment was repeated when low values of pressure strength were observed for the following specimens: (GG8_1a), (GG8_3a), (GG12_2a), (GG14_2a), (GG14_2w). GGBFS is a pozzolanic material.

Table 4.2. Compressive Strength and unit weights of GGBFS geopolymer paste.

Codes	Compressive strength (MPa)		Codes	Compressive strength (MPa)	
	2 days	28 days		2 days	28 days
GG_A	5.8	38.6	GG_W	0	21.8
GG6_1a	9.5	32.5	GG8_1w	7.7	31.4
GG6_2a	14.4	33.1	GG8_2w	8.8	29.4
GG6_3a	22.3	42.7	GG8_3w	22	27.7
GG8_1a	13	34.1	GG12_1w	18.2	35.2
GG8_2a	43	46.9	GG12_2w	17.9	38.4
GG8_3a	42.65	43.7	GG12_3w	14.7	36
GG12_1a	18	39.7	GG14_1w	33.4	41
GG12_2a	31.45	41.8	GG14_2w	28.65	26.95
GG12_3a	24.9	37.3	GG14_3w	19.9	15.4
GG14_1a	40.6	35.8	GG16_1w	25.2	31.3
GG14_2a	33.45	35	GG16_2w	25.9	29.8
GG14_3a	29.2	31.2	GG16_3w	25.7	33.7
GG16_1a	32.2	36.7	GG6_1w	7.5	33.6
GG16_2a	30.5	32.6	GG6_2w	13.3	37
GG16_3a	30	32.4	GG6_3w	18.8	39.1

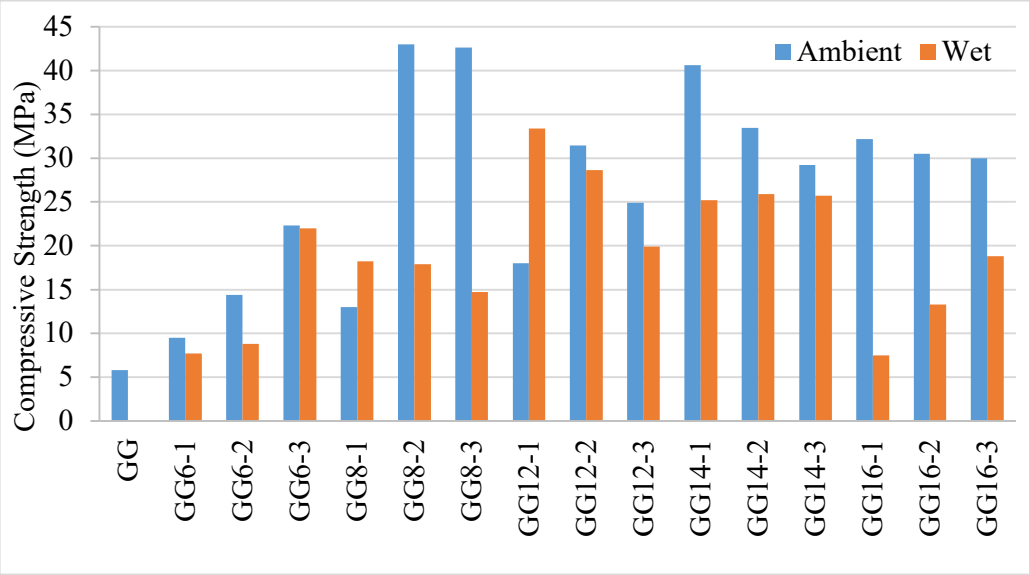

Figure 4.5. Compressive Strength (MPa) values of GGBFS-based GPs for ambient curing and wet curing conditions at 2nd day.

According to Figure 4.5,

- The highest compressive strength achieved was 43 MPa under ambient curing conditions at 80 ºC for 2 hours, whereas the compressive strength declined with rising the curing temperature, reaching 30 MPa at 160 °C for 3 hours.
- In this study, the optimum curing temperature and time is determined as 80 ºC and 2 hours.
- The minimum compressive strength for the 2nd day ambient curing is obtained on the GG reference GPs as 5.8 MPa. However, the compressive strength for the 2nd day on the reference samples in wet condition couldn't achieved.
- Ambient curing conditions for 2nd day after the heat curing is the most efficient regime for the GGBFS-based GPs.

It was observed that with increasing curing temperature, there was a corresponding reduction in compressive strength, resulting in a minimum value of 7.5 MPa.

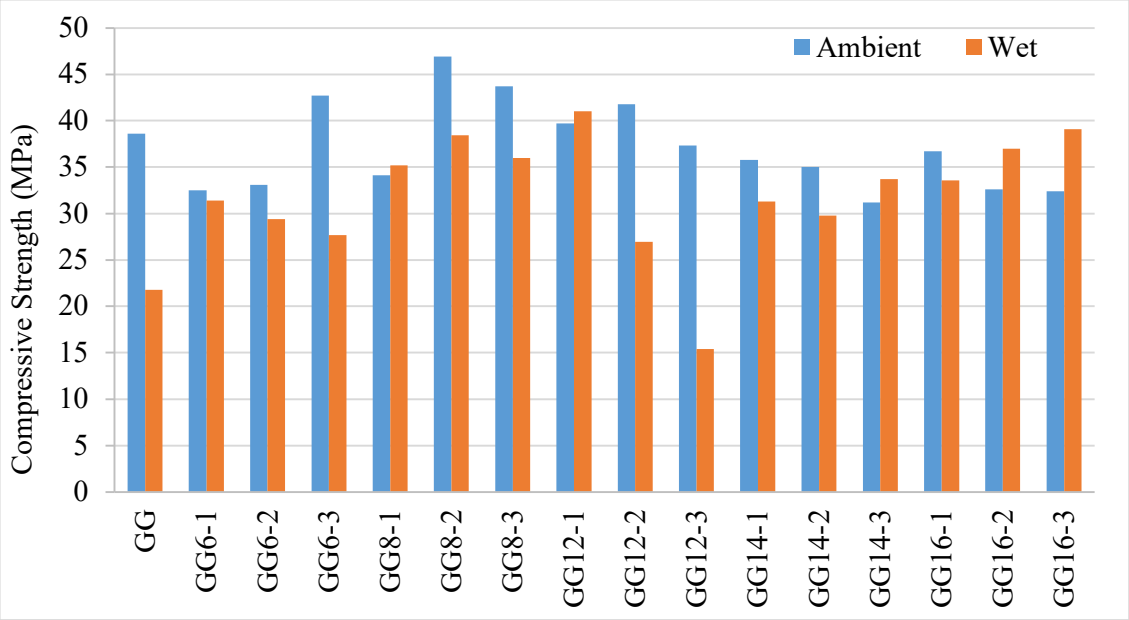

Figure 4.6. Compressive Strength (MPa) values of GGBFS-based GPs for ambient curing and wet curing conditions at 28th day.

According to Figure 4.6,

- The highest compressive strength value achieved was 46.9 MPa under ambient curing conditions at 80 ºC for two hours, whereas the compressive strength gradually declined as the curing temperature rose, reaching 31 MPa at 140 °C.
- The compressive strength value was relatively low during wet curing, measuring 21 MPa when cured without an oven. However, the highest value recorded was 41 MPa when cured at 120 °C for one hour.
- The highest compressive strength value reached 43 MPa when curied for two hours at a temperature of 80 ºC under dry curing conditions.
- Compressive strength values of GGBFS-based GP being higher when wet-cured at 160 °C for 28 days compared to dry curing is unexpected and contrary to typical behavior.

The higher temperature may promote the reactions, leading to the generation of additional strength-contributing compounds. Wet curing ensures that the concrete remains consistently moist during the curing period. This constant moisture can be beneficial for the geopolymerization process and the overall development of compressive strength. Dry curing, on the other hand, can result in evaporation of water from the concrete, potentially affecting the quality of the geopolymer structure. Curing temperature and wet conditions can accelerate the geopolymerization process. The elevated temperature may promote the reactions, leading to the development of a more robust and densely structured geopolymer gel, which results in higher compressive strength [116].

4.4. WATER ABSORPTION TEST RESULTS AND DISCUSSIONS

Water absorption test was performed according to ASTM C20. After 28 days of manufacture, cubes of paste measuring 50 mm x 50 mm x 50 mm were used to test the water absorption. The outcomes of the apparent porosity (%) and water absorption (%) of the geopolymer paste at 28 days are presented in Figures 4.7-4.10. The findings for batches that contained 10 percent of 10 moles are described. Subsequently, the outcomes of experiments that utilized MEROS are elaborated upon and the water

absorption and apparent porosity outcomes are compared. The duration of the treatment was 24 hours (submerged in water) followed by 24 hours in an oven. This can reduce UW by introducing more air spaces.

According to Figure 4.7,

- The highest water absorption values of GBFS-based GP achieved was 110.15 % under ambient curing conditions at 60 ° C for 3 hours.
- In wet group the water absorption values of GBFS-based GP gradually declined as the curing temperature rose, reaching 9 % at 160 ° C.
- In ambient group the water absorption values of GBFS-based GP slowly gradually increased even more as the curing temperature rose, reaching 59.6 % at 160 ° C.
- In wet group when specimens subjected to a temperature of 120 for two hours or more, and also at 140 ° C, the samples sustained damage, failed the test, and produced a value of 0 %.
-

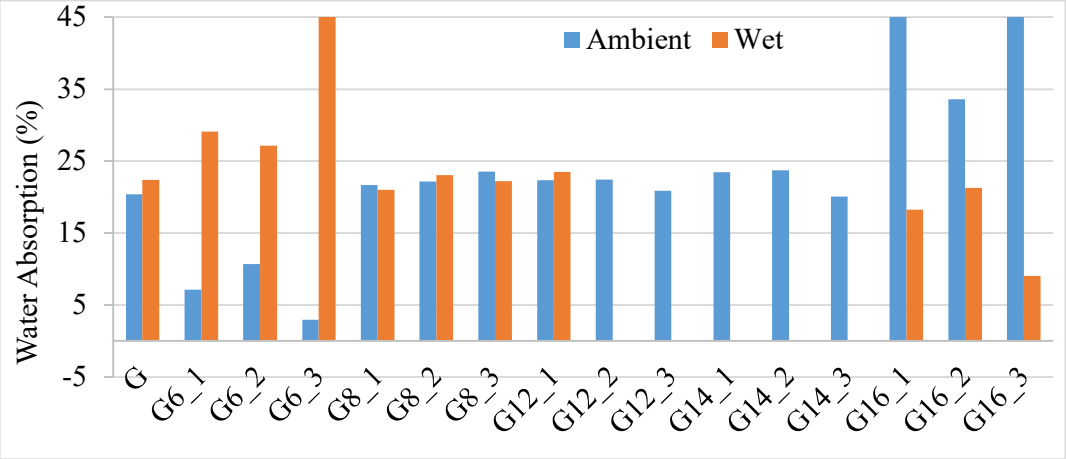

Figure 4.7. Water Absorption (%) values of GBFS-based GPs for ambient curing and wet curing conditions at 28th day.

In ambient curing, the concrete is cured at the normal environmental conditions, typically at room temperature and atmospheric humidity. This can lead to a slower curing process. In GPC with low water absorption, the limited moisture ingress reduces the risk of freeze-thaw damage [117]. GP with low water absorption tends to have a

longer service life compared to concrete with higher water absorption values. The reduced porosity minimizes the ingress of harmful substances, leading to less deterioration and maintenance over time.

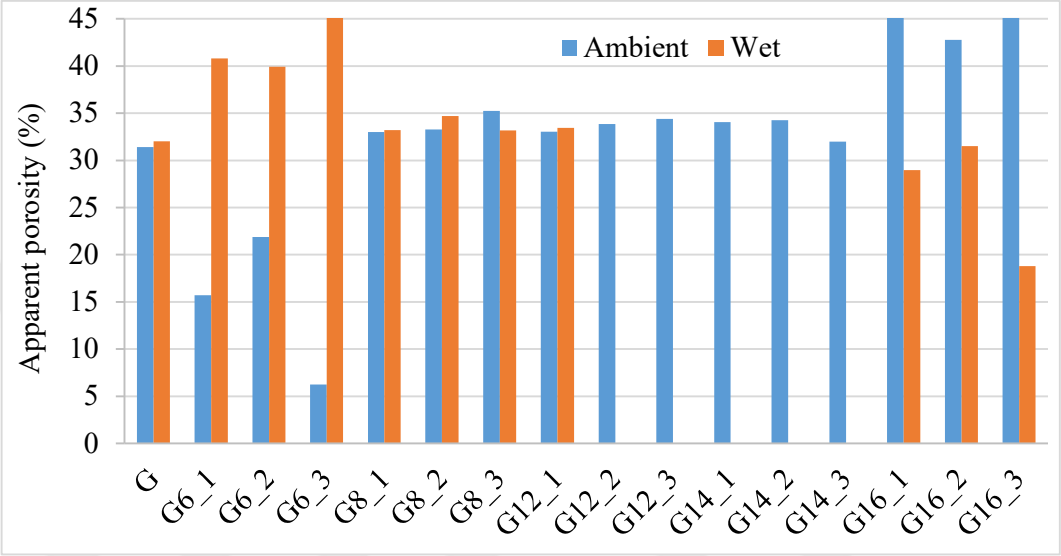

Figure 4.8. Apparent Porosity (%) values of GBFS-based GPs for ambient curing and wet curing conditions at 28th day.

According to Figure 4.8,

- The highest apparent porosity values of GBFS-based GP achieved was 80.36 % under wet curing conditions at 60 ° C for 3 hours.
- The porosity value of cured specimen at 80 ° C ranged between 30 and 35 %. The cured specimen at 120 ° C and 140 ° C and exposed to humidity suffered significant damage and failed the porosity test.
- In wet group the apparent porosity values of GBFS-based GP gradually declined as the curing temperature rose, reaching 18.8 % at 160 ° C for 3 hours.
- In ambient group the water absorption values of GBFS-based GP slowly gradually increased even more as the curing temperature rose, reaching 55.5 % at 160 ° C for 1 hour.

Porosity levels in GBFS-based GP are higher after 28 days of ambient curing due to variations in moisture content and slower curing rates. GP cured under ambient

conditions have porosity levels that are more variable and potentially higher, which could impact its long-term durability in harsh environments. ambient curing is a crucial property that reflects the concrete's pore structure and its ability to resist the ingress of water and other potentially damaging substances [118].

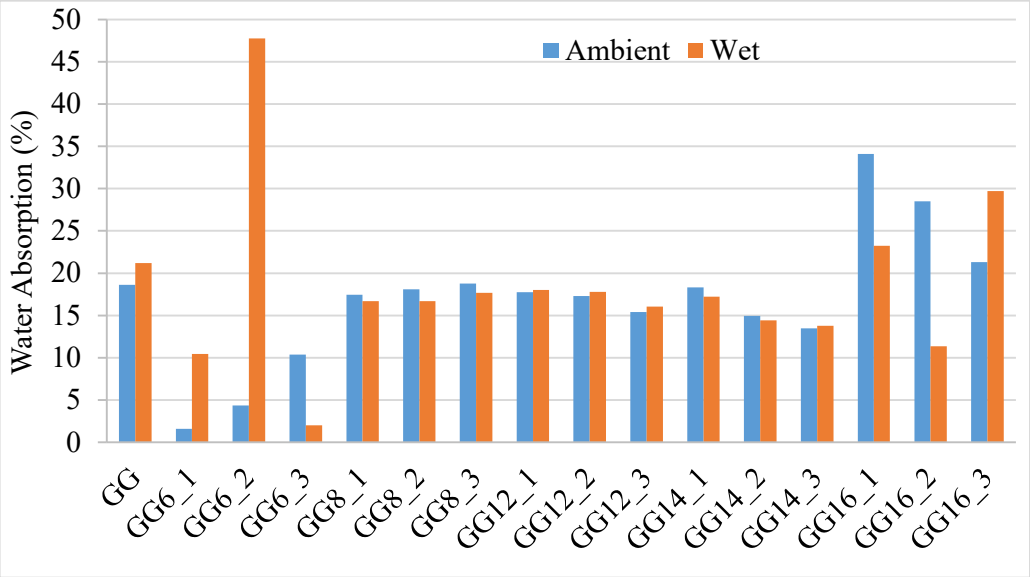

Figure 4.9. Water Absorption (%) values of GGBFS-based GPs for ambient and wet curing conditions at 28th day.

According to Figure 4.9,

- The highest water absorption values of GGBFS-based GP achieved was 47.7 % under wet curing conditions at 60 º C for 2 hours.
- In ambient group the water absorption values of GGBFS-based GP slowly gradually increased even more as the curing temperature rose, reaching 34.1 % at 160 ° C for 1 hour.
- The lowest water absorption values of GGBFS-based GP achieved was 1.5 % under ambient curing conditions at 60 º C for 1 hour.

The water absorption values of GGBFS-based GP vary depending on the curing conditions and temperature. Under ambient curing conditions, the range is a minimum

of 1.5 %. For wet curing conditions, the range is a minimum of 2 %. GP with low water absorption is generally more durable.

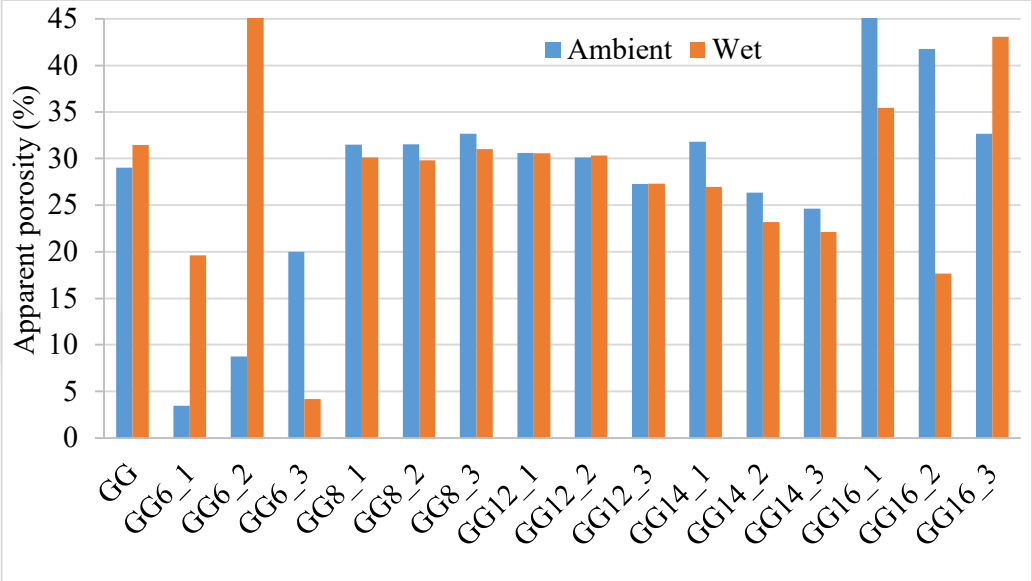

Figure 4.10. Apparent Porosity (%) values of GGBFS-based GPs for ambient and wet curing conditions at 28th day.

According to Figure 4.10,

- The highest apparent porosity values of GGBFS-based GP achieved was 67.29 % under wet curing conditions at 60 ° C for 2 hours.
- The lowest apparent porosity values of GGBFS-based GP achieved was 3.47 % under ambient curing conditions at 60 ° C for 1 hour.
- In ambient group the apparent porosity values of GGBFS-based GP slowly gradually increased even more as the curing temperature rose, reaching 47.3 % at 160 ° C for 1 hour.

The difference in apparent porosity values between GGBFS-based GP cured under ambient conditions and those cured with wet curing is primarily attributed to the consistency of moisture levels [119]. Wet curing tends to result in lower porosity due to sustained hydration.

The moisture levels in ambient curing can fluctuate based on environmental conditions. This can affect the hydration process and result in varying porosity levels. Wet curing ensures that mortar remains consistently saturated with moisture, promoting complete hydration and potentially reducing porosity.

Wet curing generally enhances the durability of concrete by reducing porosity and increasing the material's resistance to factors like chemical attack and freeze-thaw cycles. Wet curing tends to result in lower porosity levels because the consistent moisture supply facilitates more complete cementitious reactions, reducing voids and porosity. (G12_2W) (G12_3W) (G14_1W) (G14_2W) (G14_3W) samples prepared by using a percentage of GGBFS and were pre-moistened for 28 days failed in the absorption and porosity test, as shown in figure 4.15 and figure 4.16, which is due to its microstructure and the expansion of its pores, which led to a high rate of water absorption and saturation of all voids with water and thus its disintegration. Figure 4.18 shows the damage to the sample before it is completely destroyed after immersion for 24 hours.

Figure 4.11. GBFS-Wet samples at 140 °C before immersing in water

GGBFS-based GP with low water absorption is less prone to efflorescence, which is the formation of white, powdery deposits on the concrete's surface. This helps maintain the concrete's aesthetic appearance over time. Also exhibits enhanced durability and longevity due to its reduced porosity and better resistance to various environmental and chemical factors.

4.5. MICROSTRUCTURAL AND MINERALOGICAL ANALYSES

4.5.1. SEM Analyses

Scanning electron microscopy (SEM) images for the specific geopolymer pastes such as high and low compressive strength pastes are shown in Figures 4.12 - 4.17.

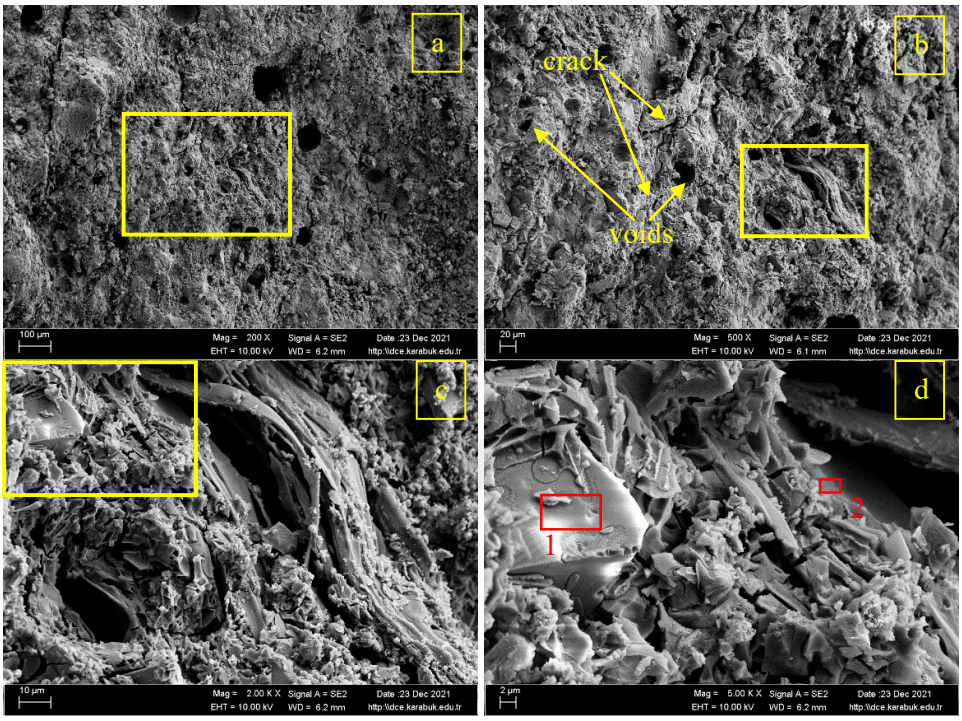

Spectrum	C	O	Na	Mg	Al	Si	S	Ca	Fe
1	15.04	56.25	3.53	4.10	4.54	10.17	0.38	5.72	0.27
2	40.36	43.84	6.33	1.47	1.60	3.45	0.53	1.89	0.53

Figure 4.12. SEM images and EDS spectrum of Reference GGBFS-based GP in wet curing

In Figure 4.12, the yellow color rectangular lines are the illustration of the next enlarged image area. Some macro voids and cracks can be seen on the SEM images in Figure 4.12a-b. Voids are smaller than 100 micron like capillary voids, but also some entrapped air voids are observed on the images. Most of the matrix is zeolitic, so these are geopolymer structures. The dust on the images did not bind, and the EDS #2 explores the carbonate structure on the GP in wet conditions. Especially Na_2CO_3 are

observed on the surfaces of the GPs in wet conditions based on the EDS spectrum analysis. The 28 days compressive strength of this specimen is achieved as 21.8 MPa. This is almost half of the maximum compressive strength value.

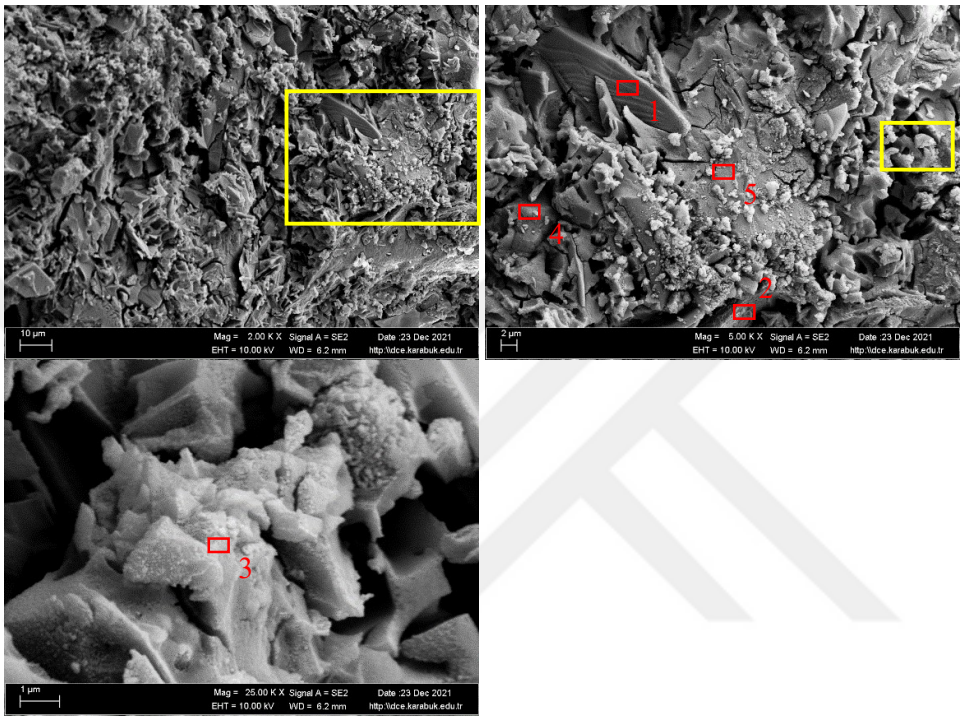

Spectrum	C	O	Na	Mg	Al	Si	S	Ca	Fe
1	12.71	40.93	3.18	5.13	6.76	17.08	1.30	12.84	0.07
2	0.00	63.79	13.93	2.87	5.49	0.00	2.29	11.62	0.00
3	16.75	53.98	6.69	2.51	2.58	9.82	0.57	6.36	0.74
4	16.05	54.18	7.16	2.41	3.21	9.46	0.55	6.38	0.60
5	16.92	54.79	6.18	3.54	3.69	9.69	0.56	4.50	0.12

Figure 4.13. SEM images and EDS spectrum of reference GGBFS-based GP in wet curing in the laboratory.

According to Figure 4.13, almost the whole body of the GP contains mostly carbonate structures based on the EDS analysis. This analysis proved by the EDS #3-5. Almost 70% of the structures have C and O atoms. However, when the carbon is emitted from the spectrum, C(N)-A-S-H forms are obtained. Based on the SEM images these are similar to the zeolitic forms because of the macroporous structures. The SiO_2/Al_2O_3 ratios of the matrix are calculated as 1.49 - 3.8. According to Deghani (2021), the maximum compressive strength is obtained for a SiO_2/Al_2O_3 ratio of 3.37. EDS#1

point is likely GGBFS particle. EDS#5 is the main geopolymer matrix form as N(C)-A-S-H with small amount of SO_4.

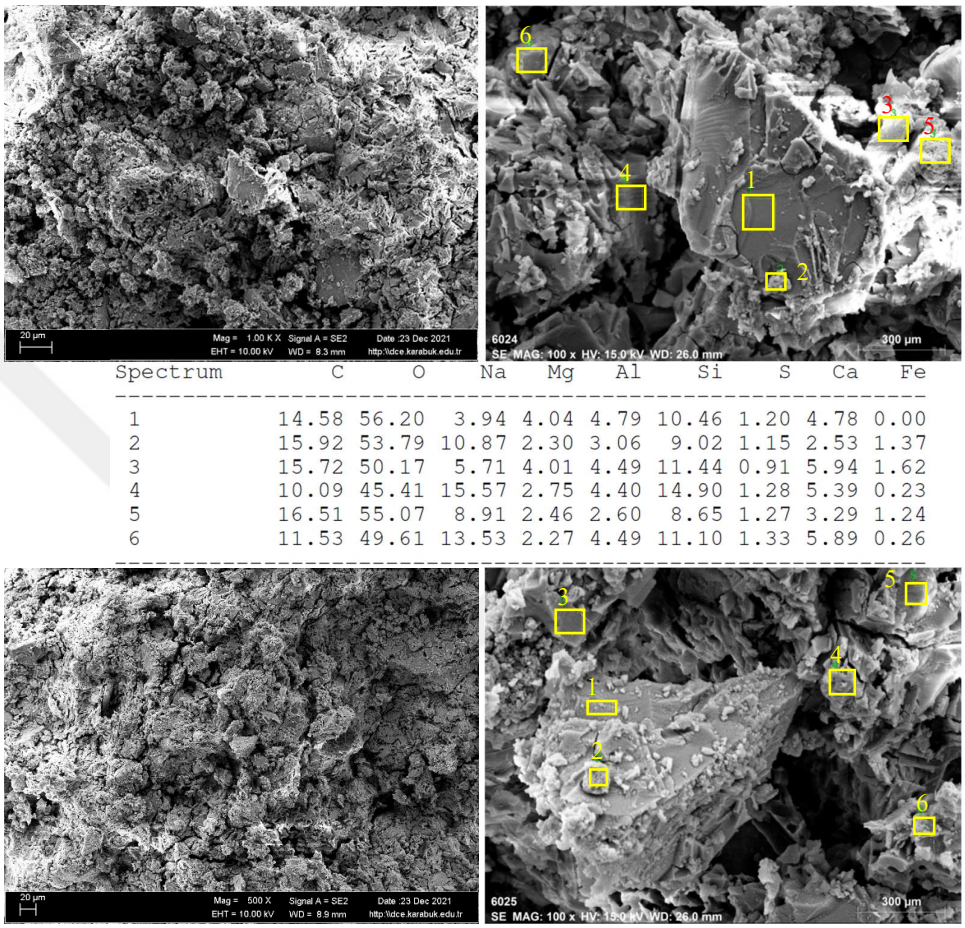

Spectrum	C	O	Na	Mg	Al	Si	S	Ca	Fe
1	14.58	56.20	3.94	4.04	4.79	10.46	1.20	4.78	0.00
2	15.92	53.79	10.87	2.30	3.06	9.02	1.15	2.53	1.37
3	15.72	50.17	5.71	4.01	4.49	11.44	0.91	5.94	1.62
4	10.09	45.41	15.57	2.75	4.40	14.90	1.28	5.39	0.23
5	16.51	55.07	8.91	2.46	2.60	8.65	1.27	3.29	1.24
6	11.53	49.61	13.53	2.27	4.49	11.10	1.33	5.89	0.26

Spectrum	C	O	Na	Mg	Al	Si	S	Ca	Fe
1	13.37	53.42	7.15	3.84	4.59	11.65	0.77	4.79	0.43
2	15.98	55.60	9.00	1.69	2.50	9.32	0.90	5.01	0.00
3	8.83	44.96	9.87	2.36	2.72	22.06	0.95	8.26	0.00
4	15.31	50.54	14.66	1.34	3.19	10.06	1.48	3.43	0.00
5	1.92	27.74	5.35	0.00	0.42	28.29	1.88	34.40	0.00
6	16.09	52.63	10.99	2.09	3.55	10.14	0.73	3.54	0.24

Figure 4.14. SEM images and EDS spectrum of reference GGBFS-based GP in ambient curing

According to Figure 4.14, some places of the GP contain mostly carbon or carbonate structures based on the EDS analysis. 70% of almost all surfaces of the specimen have C and O atoms. CSH, CASH, C(N)ASH type structures are also observed on the images based on the EDS analyses. Also, small amount of sulfur forms is observed on

the surface of the GPs. The 28 days compressive strength of this specimen is achieved as 38.6 MPa. This is close to the maximum compressive strength value. The SiO_2/Al_2O_3 ratios of the matrix are calculated as 2.53 - 3.73.

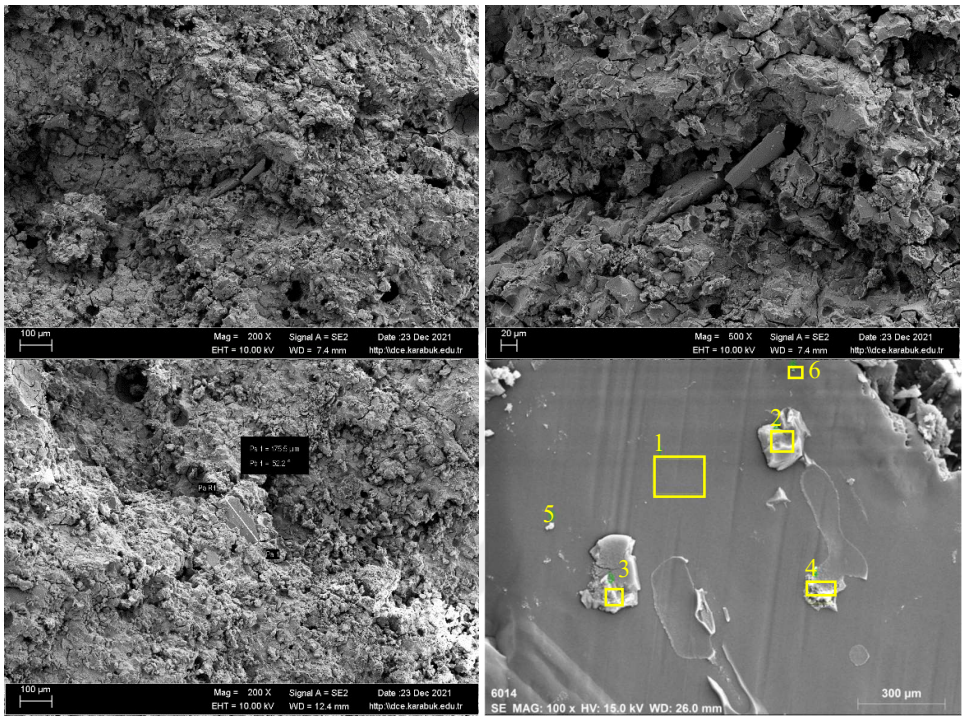

Spectrum	C	O	Na	Mg	Al	Si	S	Ca	Fe
1	40.77	7.72	0.59	0.21	0.59	49.10	0.68	0.35	0.00
2	13.42	49.87	12.61	0.98	3.26	12.92	1.32	5.62	0.00
3	15.02	53.02	6.98	1.10	2.13	10.76	0.72	10.06	0.21
4	28.45	26.78	3.11	0.54	1.03	36.78	0.65	2.27	0.39
5	31.16	31.88	4.63	2.06	1.53	25.42	1.02	1.21	1.09
6	30.40	8.38	0.85	0.30	0.78	58.03	0.69	0.34	0.24

Figure 4.15. SEM images and EDS spectrum of GGBFS-based GP 80 ºC-3h curing in ambient curing

In the SEM images of GGBFS-based GP 80 ºC-3h curing in ambient curing, the matrix has CSH and C(N)ASH. Lots of anhydrate particles are observed, however, the compressive strength is achieved as 43.7 MPa for 28 days.

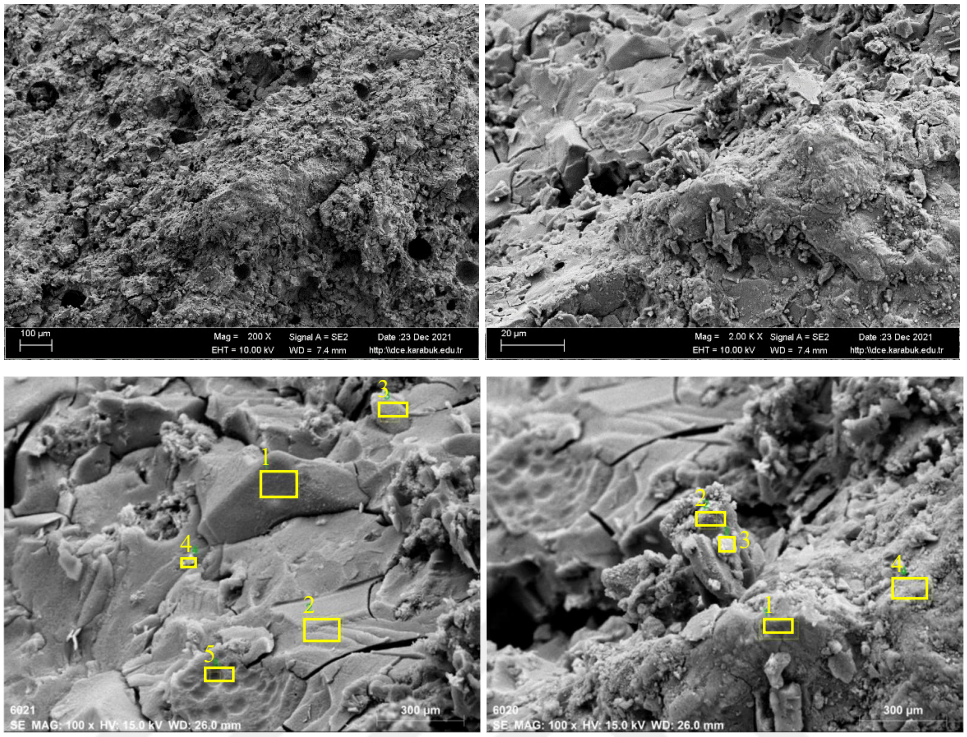

Spectrum	C	O	Na	Mg	Al	Si	S	Ca	Fe
1	13.48	38.88	2.80	5.44	6.84	15.99	1.20	13.56	1.81
2	13.00	55.22	11.24	3.33	2.96	8.35	0.87	3.80	1.23
3	12.07	52.81	2.72	5.13	5.71	12.65	0.73	7.85	0.32
4	13.71	51.30	11.88	2.52	3.12	10.09	1.21	4.72	1.45
5	78.88	19.08	1.33	0.11	0.00	0.04	0.25	0.24	0.08

Spectrum	C	O	Na	Mg	Al	Si	S	Ca	Fe
1	8.80	52.90	7.12	4.16	1.08	3.76	0.44	5.82	15.90
2	13.92	45.85	10.36	2.84	3.89	13.49	1.10	6.76	1.78
3	18.80	51.10	7.58	1.33	10.42	6.39	0.88	2.88	0.61
4	13.94	59.51	5.52	3.21	1.70	3.70	1.04	5.79	5.59

Figure 4.16. SEM images and EDS spectrum of GGBFS-based GP 120 ºC-2h curing in ambient curing

In the SEM images of GGBFS-based GP 120 ºC-2h curing in ambient curing, the matrix has CSH and C(N)ASH with sulfur. Moreover, the carbon forms cause to integration of the geopolymer structures, and so the surfaces of the GP are observed as highly rigid structures. The compressive strength is obtained as 41.8 MPa for 28 days. However, some cracks on the rigid surface are observed. It is thought that the cracks occurred because of the shrinkage.

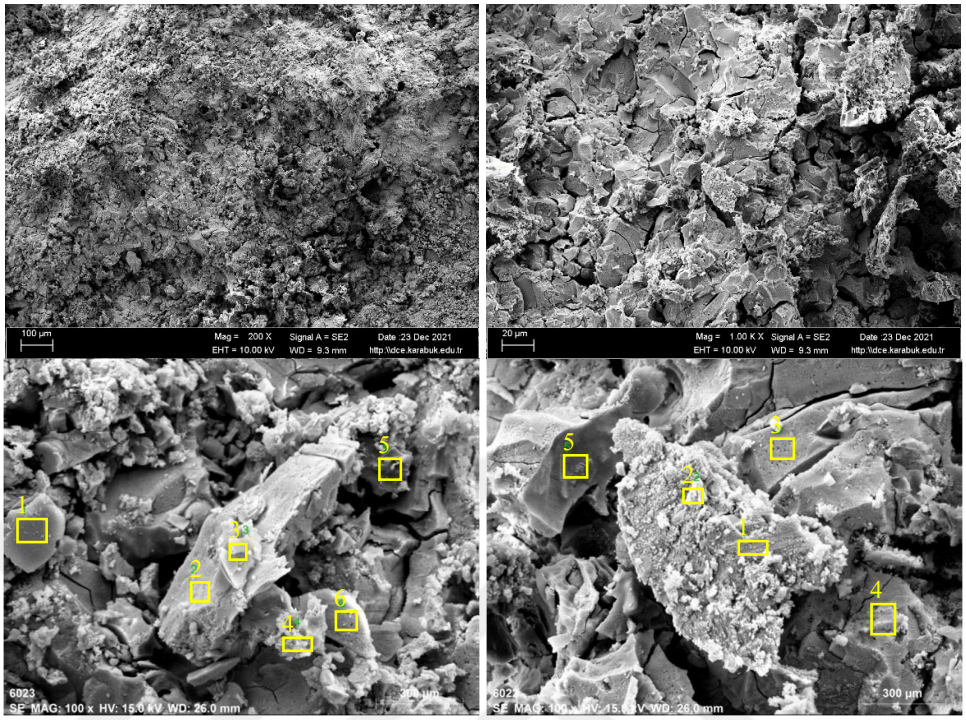

Spectrum	C	O	Na	Mg	Al	Si	S	Ca	Fe
1	77.62	18.50	2.37	0.00	0.35	0.21	0.61	0.34	0.00
2	17.67	51.20	9.54	2.30	2.48	9.83	1.22	4.34	1.42
3	70.43	24.40	2.04	0.33	0.33	1.23	0.74	0.50	0.00
4	10.55	57.00	5.97	1.31	2.78	6.23	0.73	14.87	0.56
5	60.61	28.81	4.73	0.62	0.73	1.96	1.35	1.19	0.00
6	14.32	53.85	8.56	2.86	3.00	11.10	0.62	5.67	0.00

Spectrum	C	O	Na	Mg	Al	Si	S	Ca	Fe
1	27.77	42.54	8.50	1.54	2.57	10.54	1.10	5.43	0.00
2	15.09	51.17	8.33	2.54	2.31	10.94	1.05	7.22	1.36
3	12.47	56.35	10.66	2.11	2.84	9.97	0.93	4.60	0.07
4	11.99	54.37	12.01	2.33	3.13	10.73	0.92	4.53	0.00
5	24.80	40.78	9.36	1.46	2.69	11.98	1.24	7.70	0.00

Figure 4.17. SEM images and EDS spectrum of GGBFS-based GP 160 ºC-2h for ambient curing.

According to Figure 4.17, 160 ºC curing makes more rigid the GP structures. lots of cracks are observed on the surfaces, and this is because of the thermal shrinkage. Therefore, the compressive strength of this specimen is achieved as 32.6 MPa. The structures of the specimens include C(N)ASH with carbon forms.

The amorphous or glassy structure of GBFS particles contributes to their pozzolanic reactivity when mixed with water and calcium hydroxide. The chemical composition of ground granulated blast furnace slag (GBFS) varies, but it generally contains

significant amounts of silica, alumina, and calcium oxide. These compounds contribute to GBFS's pozzolanic and hydraulic properties when employed in cementitious mixtures. GBFS particles are pozzolanic, meaning that they combine with calcium hydroxide (which is a byproduct of cement hydration) to create calcium silicate hydrate (C-S-H) gel, which serves as the principal bonding material in concrete. This pozzolanic activity enhances the concrete's strength and durability.

4.5.2. XRD Analyses

XRD analysis of the specimens are given in Figure 4.19, however the materials XRD analyses are also given in Figure 4.18. Moreover, the oxide analysis of the GP is given in Table 4.5. Based on the oxide analysis, the GP structures include mostly CaO, SiO_2, Fe_2O_3, Al_2O_3, Na_2O, MgO and Na_2SO_4.

Table 4.3. Oxide analysis of the GPs.

Code	SiO_2	Al_2O_3	Fe_2O_3	CaO	MgO	Na_2O	Na_2SO_4	H_2O
GP	21.65	6.71	7.04	24.26	6.30	6.85	4.25	20.10

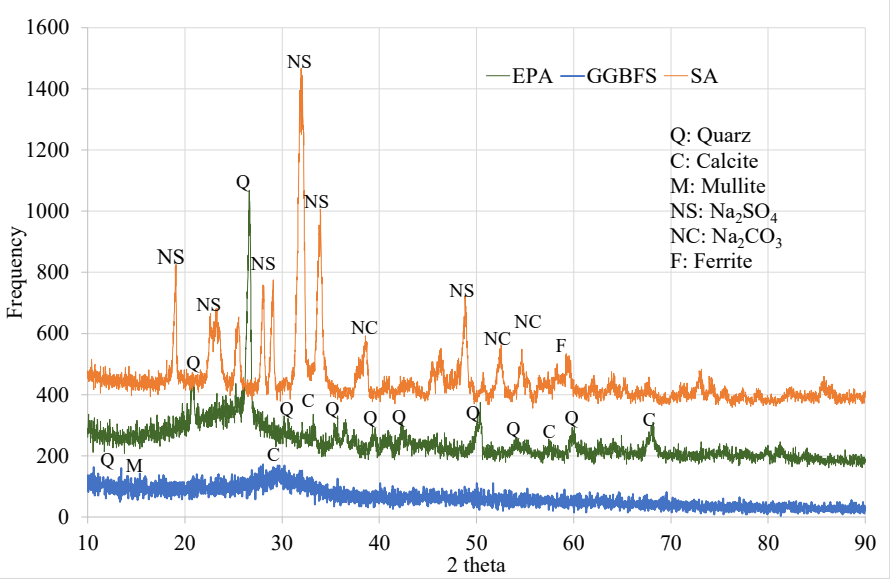

Figure 4.18. XRD analysis of materials used in GPs.

XRD analysis of the GPs, based on Figure 4.19, shows mostly the mullite form as well as quartz, CSH, and CASH forms. CASH structures are clearly observed on the GPs cured in 80 ºC and 160 ºC. however, calcite or carbonate forms are also seen on the XRD peaks. Mullite forms are lesser observed on the ambient cured GPs without heat exposure. The general structure of all GPs is seen amorphous between 20 – 40 theta.

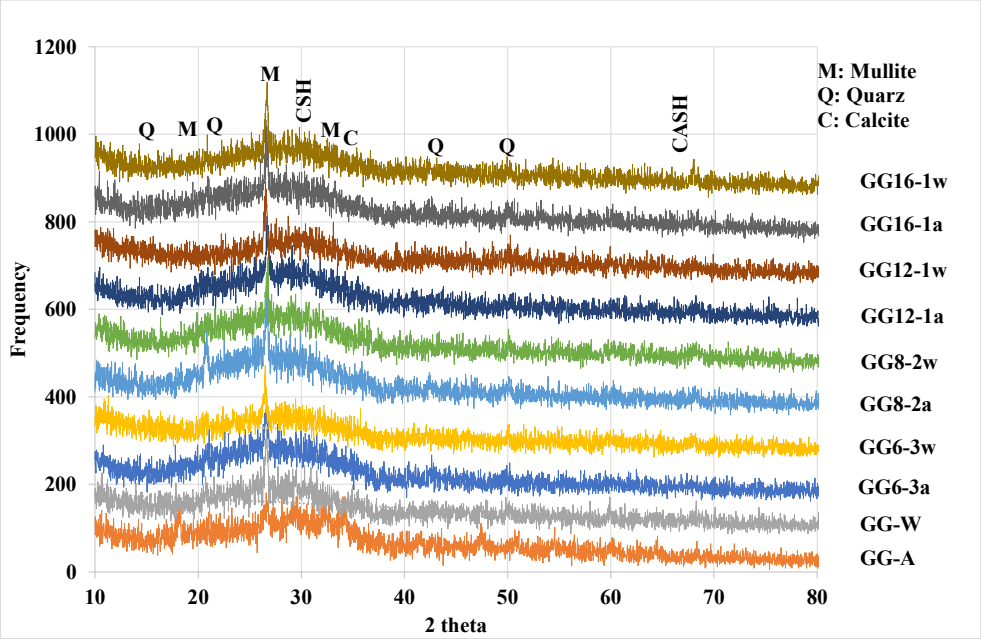

Figure 4.19. XRD analysis of produced GPs.

PART 5

SUMMARY AND CONCLUSIONS

5.1. GENERAL

Increasing energy consumption is the main problem for sustainable development in the iron and steel industry, so the latest studies focus on the possibility of benefiting from waste heat in iron and steel factories and searching for the best possible ways to make the most of these factories. The aim of this study was to determine the possibility of benefiting from waste and management activities in the iron and steel industry, where previous studies indicate that the global average of waste generated by iron and steel factories in the world is about 0.3 tons of waste generated.

The silica and alumina source derived from the Energy Transferring System Ash, ground granulated blast furnace slag (GGBFS) and granular blast furnace slag (GBFS). A mixture of sodium silicate (Na_2SiO_3) and sodium hydroxide (NaOH) was used as an alkaline source. Workability, physical properties, and mechanical qualities were improved using MEROS in this investigation. We have run flow table test on every batch of mixes we make. The compressive strength test was performed at 2 and 28 days. In addition, on 28^{th} day, water absorption test was performed on all mix samples.

5.2. CONCLUSION

To conclude, the conducted experimental research on various combinations of ground granulated blast furnace slag (GBFS) and ground granulated blast furnace slag (GGBFS) in geopolymer concrete has yielded significant findings on their flow attributes, unit weights, and ability to withstand compressive strength in differing conditions of curing. The unit weights of the geopolymer concretes based on both

GBFS and GGBFS depend heavily upon the curing temperature and the method applied.

After experimental research conducted, the following conclusions and notes can be expressed:

- Mixtures containing GGBFS have relatively low flowability because of high cohesiveness and specific surface.
- The lowest and highest unit weights (UW) of the GBFS-based GPs are 1.55 g/cm^3 and 2.2 g/cm^3, respectively. While the highest UW is observed on the ambient -cured GPs at 140 ºC, the lowest UW is on the wet-cured GPs at 80 ºC.
- The lowest and highest unit weights (UW) of the GGBFS-based GPs are 1.75 g/cm^3 and 2.1 g/cm^3, respectively. While the highest UW is observed on the ambient-cured GPs at 80 ºC, the lowest UW is on the wet-cured GPs at 60 ºC.
- The highest and lowest early compressive strength of the GPs are 3.6 MPa and 2.5 MPa respectively for the ambient-cured GBFS-based GPs. However, on the GGBFS-based GPs, the highest and lowest early compressive strength are 42.65 MPa and 5.8 MPa respectively.
- The highest and lowest late compressive strength of the GPs are 13.3 MPa and 2 MPa respectively for the ambient-cured GBFS-based GPs. However, on the GGBFS-based GPs, the highest and lowest late compressive strength are 46.9 MPa (with ambient curing) and 15.4 MPa (with wet curing) respectively.
- The optimal curing temperature for the slag/EPA-based GPs is 80 °C followed by ambient (dry) curing. XRD analysis reveals the clear presence of calcium aluminium silicate hydrate (CASH) structures in the geopolymer samples cured at 80 °C and 160 °C. This indicates that temperature plays a crucial role in the formation of CASH phases, establishing a correlation between heat exposure and the crystalline structure of the geopolymer matrix.
- The wet curing effects negatively to the early and late compressive strength values of the both GBFS and GGBFS-based GPs.

- GGBFS mixtures with chemical additives from MEROS work on increasing its cohesion as the fine granules fill the voids, which reduces absorption and increases compressive strength.
- The curing conditions significantly influenced the apparent porosity levels of GBFS-based geopolymer concretes (GP). The material's pore structure was notably affected by moisture and temperature, as evidenced by the highest apparent porosity of 80.36% observed during wet curing conditions at 60°C for 3 hours. The porosity values of specimens cured at 80 °C ranged from 30% to 35%. However, specimens exposed to higher temperatures (120 °C and 140 °C) and humidity sustained damage, resulting in test failure.
- For GGBFS-based GP, the maximum water absorption of 47.7% was observed during wet curing at 60 °C for two hours. In contrast, the material had the minimum water absorption of 1.5% when cured at 60 °C for an hour in ambient conditions. The visible porosity of GGBFS-based GP was between 3.47% and 67.29%.

Furthermore, this study highlights the negative impact of wet curing on the compressive strength of GBFS and GGBFS-based concretes.

Moreover, the introduction of chemical additives from MEROS into GGBFS mixtures is shown to enhance cohesion by filling voids, reducing absorption, and ultimately improving compressive strength values.

These findings provide a more profound insight into the mechanical properties of geopolymer concretes with diverse slag compositions and curing conditions. They can assist in selecting suitable mixtures and curing techniques for specific applications, promoting the use of sustainable and eco-friendly construction materials.

5.3. SUGGESTED RECOMMENDATIONS FOR FUTURE STUDIES IN THIS FIELD

In order to reach better and more accurate results, and after considering the results which is obtained from this study, some recommendations could be made for other future studies;

1) The Granulated blast furnace slag used in this study has a limit range in in the geopolymer mixture. where it has a low-pressure resistance and poor adsorption resistance, as a result of this, the further studies should be continued with using diverse type of slags.

2) A limited number of specimens were tested in this study. Therefore, it is suggested to increase the number of specimens for compressive strength and absorption tests.
3) It is suggested to try temperatures more than 160 °C, which is the maximum temperature were samples tested due to laboratory conditions.

4) In this study, the compressive strength test was performed after 2 and 28 days. So, it is suggested to make the compressive strength test on multiple days such as 7 and 90 days in order to confirm the results.

REFERANCES

1. Amer, I., Kohail, M., El-Feky, M. S., Rashad, A., & Amera, M. A. K. I. (2021). A review on alkali-activated slag concrete. Ain Shams Engineering Journal, 12, 1475–1499.

2. Bilim, C., & Atiş, C. D. (2011). The abrasion and strength properties of mortars containing ground granulated blast furnace slag. Journal of Polytechnic, 14, 101–104.

3. Davidovits, J. (2002). 30 years of successes and failures in geopolymer applications. Market trends and potential breakthroughs. Geopolymer 2002 Conference, 3–7.

4. MA, C. J., Guang-yu, Z., Wen-wei, Z., & DONG, A. (2012). Analytical research on waste heat recovery and utilization of China's iron & steel industry. Energy Procedia, 16, 1023–1025.

5. Abdel-Gawwad, H. A., & Abo-El-Enein, S. A. (2019). A novel method to produce dry geopolymer cement powder. HBRC Journal, 15, 1687–4048.

6. Anuradha, R., et al. (2011). Modified guidelines for geopolymer concrete mix design using Indian standard. Asian Journal of Civil Engineering, 12, 353–364.

7. Franco Muleya, H. K. (2017). An investigation of waste management practices in the Zambian construction industry. Journal of Building Construction and Planning Research, 5, 1–13.

8. Luhar, S., Luhar, I., Nicolaides, D., & Gupta, R. (2021). Durability performance evaluation of rubberized geopolymer concrete. Sustainability, 13, 1–3.

9. Eren, E., Derun, M. M., & Pişkin, S. (2018). Investigation of the effects of boric acid and boric acid waste on the alkaline activation of blast furnace slag. Sigma Journal of Engineering and Natural Sciences, 36, 480–485.

10. A, Y. S., O, P. A., & Somerset, V. (2021). A decision-support framework for industrial waste management in the iron and steel industry: A case study in Southern Africa. Case Studies in Chemical and Environmental Engineering.

11. Taher, S. M. S., Saadullah, S. T., & Tayeh, B. A. (2021). Behavior of geopolymer concrete deep beams containing waste aggregate of glass and limestone as a partial replacement of natural sand. Case Studies in Construction Materials, 15, 2021.

12. Wongkvanklom, A. P. P. K. T. K., & Chindaprasirt, P. (2021). Beneficial utilization of recycled asphaltic concrete aggregate in high calcium fly ash geopolymer concrete. Case Studies in Construction Materials, 14, 2021.

13. Sarmin, S. N., Welling, J., Krause, A., & Shalbafan, A. (2014). Investigating the possibility of geopolymer to produce inorganic-bonded wood composites for multifunctional construction material – A review. BioResources, 9, 1–5.

14. Thomas, R. J., Ye, H., Radlińska, A., & Others. (2016). Alkali-activated slag cement concrete. Concrete International: Design & Construction, 38, 34.

15. Wu, J., Min, Y., Li, B., & Zheng, X. (2021). Stiffness and strength development of the soft clay stabilized by the one-part geopolymer under one-dimensional compressive loading. Soils and Foundations, 61(4), 974–988.

16. Sajan, P., Jiang, T., Lau, C., Tan, G., & Ng, K. (2021). Combined effect of curing temperature, curing period and alkaline concentration on the mechanical properties of fly ash-based geopolymer. Clean Technologies and Environmental Policy, 1–10.

17. Mudgal, M., Singh, A., Chouhan, R. K., Acharya, A., & Srivastava, A. K. (2021). Fly ash red mud geopolymer with improved mechanical strength. Clean Energy, 5, 100215.

18. Abd El-Gawad, H., & Aboul-Enein, A. (2019). A novel method to produce dry geopolymer cement powder. HBRC Journal, 15, 13–24.

19. Hakem, I., et al. (2018). The characterization of steel slag by alkali activation. Open Access Library Journal, 5, 1–14.

20. Zidi, I. Z. (2020). Characterization of Nano-Silica Local Metakaolin Based-Geopolymer: Microstructure and Mechanical Properties. Open Journal of Civil Engineering, 10, 143–161.

21. Mehta, P. K. (2010). Sustainable cements and concrete for the climate change era – A review. Proceedings of the 2nd International Conference on Sustainable Construction Materials and Technologies, 1, Ancona, Italy, June 28-30.

22. Davidovits, J. (2013). Geopolymer Cement: A Review. Published in Geopolymer Science and Technics, Technical Paper #21, Geopolymer Institute Library.

23. Mohsen, A., Aiad, I., El-Hossiny, F. I., & Habib, A. O. (202). Evaluating the Mechanical Properties of Admixed Blended Cement Pastes and Estimating its Kinetics of Hydration by Different Techniques. Egyptian Journal of Petroleum.

24. Rowles, M., & O'Connor, B. (2003). Chemical optimization of the compressive strength of aluminosilicate geopolymers synthesized by sodium silicate activation of metakaolinite. Journal of Materials Chemistry, 13(6), 1161–1165.

25. Davidovits, J. (2014). Geopolymer Chemistry and Applications, 3rd ed. Geopolymer Institute.

26. Jimenez, A. F., Palomo, A., & Criado, M. (2005). Microstructure Development of Alkali-activated Fly ash cement: A descriptive Model. Cement and Concrete Research, 35, 1204-1209.

27. Davidovits, J., Buzzi, L., Rocher, P., Marini, D. G. C., & Tocco, S. (1999). Geopolymeric cement based on low-cost geologic materials – geosystem. In: Second International Conference Geopolymer 99, France.

28. Davidovits, J. (2018). Why Alkali-Activated Materials (AAM) are Not Geopolymers, Technical Paper #25, Geopolymer Institute Library. Retrieved from www.geopolymer.org.

29. Tognonvi, J. S. and Tohoué, S. R. Monique. (2012). Durability of Tubular Geopolymer Reinforced with Silica Sand. New Journal of Glass and Ceramics, pp. 85–90.

30. Palomo, A., Krivenko, P., Garcia-Lodeiro, I., Kavalerova, E., Maltseva, O., & Fernández Jiménez, A. (2014). A review on alkaline activation: new analytical perspectives. Materials and Structures, 64(315), e022.

31. Purdon, A. O. (1940). The action of alkalis on blast-furnace slag. Journal of the Society of Chemical Industry, 59(9), 191–202.

32. Glukhovsky, V. D. (1967). Soil Silicate Articles and Structures. Budivelnyk Publisher, Kiev. (in Ukrainian). [33] Davidovits, J. (1984). Synthetic mineral polymer compound of the silico aluminates, family and preparation process. US Patent 4472199.

33. Nenadović, S., & Vukčević, M. (2022). Structural, mechanical, and chemical properties of low content carbon geopolymer.

34. Talling, B., & Brandstetr, J. (1989). Present and future of alkali-activated slag concrete. In Proceedings of the 3rd International Conference on the Use of Fly Ash, Silica Fume, Slag & Natural Pozzolans in Concrete (pp. 1519–1546). SP-114, Norway.

35. Palomo, A., Grutzeck, M. W., & Blanco, M. T. (1999). Alkali-activated fly ashes: A cement for the future. Cement and Concrete Research, 29, 1323–1329.

36. Fernández-Jiménez, A., Palomo, A., & López-Hombrados, C. (2006). Engineering properties of alkali-activated fly ash concrete. ACI Materials Journal, 103(2), 106-112.

37. Duxson, P., Provis, J. L., Lukey, G. C., Mallicoat, S. W., Kriven, W. M., & van Deventer, J. S. J. (2005). Colloid Surf. A-Physicochem. Eng. Asp., 269(1–3), 47–58.

38. Fernández-Jiménez, A., Palomo, A., Pastor, J. Y., & Martín, A. (2008). New cementitious materials based on alkali-activated fly ash: Performance at high temperature. Journal of the American Ceramic Society, 91(10), 3308–3314.

39. Shi, C., Roy, D. M., & Krivenko, P. V. (Eds.). (2006). Alkali-activated Cements and Concretes. Taylor & Francis, London, U.K.

40. Shi, C., Fernández Jiménez, A., Krivenko, P. V., & Palomo, A. (2010). Classification and characteristics of alkali-activated cements. First International Conference on Advances in Chemically-Activated Materials (CAM'2010-China), in Conjunction with 7th International Symposium on Cement and Concrete (ISCC2010), Jinan, China.

41. Fernández-Jiménez, A., Puertas, F., Sanz, J., & Sobrados, I. (2003). Structure of calcium silicate hydrated formed in alkali-activated slag pastes: Influence of the type of alkaline activator. Journal of the American Ceramic Society, 86(8), 1389–1394.

42. Ferdous, M. W., Kayali, O., & Khennane, A. (2013). A detailed procedure of mix design for fly ash-based geopolymer concrete. In Fourth Asia-Pacific Conference on FRP in Structures, Australia.

43. Patankar, S. V., Ghugal, Y. M., & Jamkar, S. S. (2014). Effect of concentration of sodium hydroxide and degree of heat curing on fly ash-based geopolymer mortar. Indian Journal of Materials Science.

44. Shi, C., Fernández Jiménez, A., & Palomo, A. (2011). New cements for the 21st century: The pursuit of an alternative to Portland cement. Cement and Concrete Research, 41(7).

45. Yao, X., Zhang, Z., Zhu, H., & Chen, Y. (2009). Geopolymerization process of alkali–metakaolinite characterized by isothermal calorimetry. Thermochimica Acta, 493, 49–54.

46. Gong, Y. F., Fang, Y. H., Yan, Y. R., & Chen, L. Q. (2014). Investigation on alkali-activated recycled cement mortar powder cementitious material. Materials Research Innovations, 18(2), 784–787.

47. Yahya, Z., Abdullah, M. M. A. B., Hussin, K., Ismail, K. N., Razak, R. A., & Sandu, A. V. (2015). Effects of solids-to-liquids, Na2SiO3-to-NaOH, and curing temperature on the palm oil boiler ash (Si+Ca) geopolymerization system. Materials, 8, 2227–2244.

48. Payá, J., Agrela, F., Rosales, J., Morales, M. M., & Borrachero, M. V. (2019). Application of alkali-activated industrial waste. In J. de Brito & F. Agrela (Eds.),

New Trends in Eco-efficient and Recycled Concrete (pp. 357–424). Woodhead Publishing.

49. Mangat, P., & Lambert, P. (2016). Sustainability of alkali-activated cementitious materials and geopolymers. In J. M. Khatib (Ed.), Sustainability of Construction Materials (Second Edition) (pp. 459–476). Woodhead Publishing.

50. Manjunath, R., & Narasimhan, M. C. (2020). Alkali-activated concrete systems: A state of the art. In P. Samui, D. Kim, N. R. Iyer, & S. Chaudhary (Eds.), New Materials in Civil Engineering (pp. 459–491). Butterworth-Heinemann.

51. Mahdieh, K., Hani, A., Yong-Rak, K., Gabriel, N., & Sussan. (2018). Effects of Na2O/SiO2 molar ratio on properties of aggregate-paste interphase in fly ash-based geopolymer mixtures through multiscale measurements. Construction and Building Materials, 191, 564–574.

52. Mehta, P. K. (1987). Natural pozzolans: Supplementary cementing materials in concrete. CANMET Special Publication.

53. Snellings, R., Mertens, G., & Elsen, J. (2012). Supplementary cementitious materials. Reviews in Mineralogy and Geochemistry.

54. Book, D. J. (1986). Natural pozzolanas. In Cement Replacement Materials, Surrey University Press.

55. Gibbons, P. (1997). Pozzolans for lime mortars. In The Conservation and Repair of Ecclesiastical Buildings.

56. Hanifi, B. (2007). Effect of crushed ceramic and basaltic pumice as fine aggregates on concrete mortars properties. Construction and Building Materials, ISSN 0950-0618.

57. Richards, I. G., Palmer, J. P., & Barratt, P. A. (1993). The Reclamation of Former Coal Mines and Steelworks. Richards, Moorehead & Laing Ltd. ISBN: 4444170H.

58. Rayner-Canham, & Overton (2006). Descriptive Inorganic Chemistry, Fourth Edition. New York: W. H. Freeman and Company. pp. 534–535. ISBN 978-0-7167-7695-6.

59. Thomas, G. H. (1983). Properties of iron and steel slags. In Reclamation of Former Iron and Steel works Sites, Conference Proceedings (Windermere 1983), edited by G. P. Doubleday, Cl-C8.

60. Motorwala, A., Shah, V., Kammula, R., Nannapaneni, P., & Raijiwala, D. (2008). ALKALI Activated FLY-ASH Based Geopolymer Concrete.

61. Sakulich, A. (2011). Reinforced Geopolymer Composites for Enhanced Material Greenness and Durability. Sustainable Cities and Society.

62. Pavithra, P., Reddy, M. S., Dinakar, P., Rao, B. H., Satpathy, B. K., & Mohanty, A. N. (2016). Effect of the Na2SiO3/NaOH Ratio and NaOH Molarity on the Synthesis of Fly Ash-Based Geopolymer Mortar. GeoChicago GSP 272, 336-344.

63. Mijarsh, M. J. A., Johari, M. A. M., & Ahmad, Z. A. (2015). Effect of delay time and Na2SiO3 concentrations on compressive strength development of geopolymer mortar synthesized from TPOFA. Construction and Building Materials, 86, 64–74.

64. Patil, A. A., Chore, H. S., & Dodeb, P. A. (2014). Effect of curing condition on strength of geopolymer concrete. Advances in Concrete Construction, 2(1), 29–37.

65. Abdullah, A., Hussin, K., Bnhussain, M., Ismail, K. N., & Ibrahim, W. M. W. (2011). Mechanism and Chemical Reaction of Fly Ash. International Journal of Pure and Applied Sciences and Technology, 6, 35–44.

66. Gunasekara, M. P. C. M., & Law, D. W. (2014). Proceedings of the 23rd Australasian Conference on the Mechanics of Structure and Materials, Byron Bay, Australia.

67. Duxson, P., Mallicot, S. W., Lukey, G. C., Kriven, W. M., & van Deventer, J. S. J. (2007). Colloids and Surfaces A: Physicochemical and Engineering Aspects, 292, 8–20.

68. Hardjito, D., & Rangan, B. V. (2005). Development and Properties of Low-calcium Fly Ash based Geopolymer Concrete. Research Report GC.

69. Divya, K., & Rubina, C. (2007). Mechanism of geopolymerization and factors influencing its development: A review. Journal of Materials Science, 42, 729–746.

70. Lloyd, N. A., & Rangan, B. V. (2010). Geopolymer concrete with fly ash. Second International Conference on Sustainable Construction Materials and Technologies, Ancona, Italy.

71. Anuradha, R., Sreevidya, V., Venkatasubramani, R., & Rangan, B. V. (2012). Modified guidelines for geopolymer concrete mix design using Indian Standard. Asian Journal of Civil Engineering, Building, and Housing, 13(3), 353–364.

72. Olivia, M., & Nikraz, H. (2012). Properties of fly ash geopolymer concrete designed by Taguchi method. Materials & Design, 36, 191–198. https://doi.org/10.1016/j.matdes.2011.11.013

73. David, H., Scott, S., & Kevin, E. P. (2007). The Geomorphology of the Great Barrier Reef. Oceanography.

74. Aly, Z., Vance, E. R., Perera, D. S., Davis, J., Durce, D., Hanna, J. V., & Griffith, C. S. (2008). Aqueous leachability of metakaolin-based geopolymers with molar ratios of Si/Al = 1.5 to 4. Journal of Nuclear Materials, C S.

75. ASTM International. (2002). Standard Test Methods for Determining Chemical Durability of Nuclear, Hazardous, and Mixed Waste Glasses and Multiphase Glass Ceramics: The Product Consistency Test (PCT), Designation C1285-02. West Conshohocken, PA: ASTM International.

76. Adaska, W. S., Tresouthick, S. W., & West, P. B. (1998). Solidification and stabilization of wastes using Portland cement (No. EB071.02W).

77. Gök, S. G., & Kılınç, K. (Year). Mechanical properties of fly ash and blast furnace slag-based alkali-activated concrete. Kirklareli University Journal of Engineering and Science, 3(2), 123–131.

78. Lv, Y., Wang, C., Han, W., Li, X., & Peng, H. (2023). Study of the mechanical properties and microstructure of alkali-activated fly ash–slag composite cementitious materials. Polymers (Basel), 15(8).

79. Olubusola, G. Malumbela, and O. Philip, 'Influence of chemical composition of soda ash activated fly ash and copper slag geopolymer pastes on compressive strength', vol. 11, pp. 437–446, 2023, doi: 10.5267/j.esm.2023.4.002.

80. Aziz, I. H., et al. (2017). The characterization of steel slag by alkali activation. OALib, 04(11), 1–13. https://doi.org/10.4236/oalib.1103816.

81. Collins, F. G., & Sanjayan, J. G. (1999). Workability and mechanical properties of alkali-activated slag concrete. Cement and Concrete Research, 29(3), 455–458.

82. Wattanachai, P., & Suwan, T. (2017). Strength of geopolymer cement curing at ambient temperature by non-oven curing approaches: An overview. IOP Conference Series: Materials Science and Engineering, 212(1).

83. Hassan, A., Arif, M., & Shariq, M. (2019). Effect of curing condition on the mechanical properties of fly ash-based geopolymer concrete. SN Applied Sciences, 1(12), 1–9.

84. Muhammad, N., Baharom, S., Amirah, N., Ghazali, M., & Alias, N. A. (2019). Effect of heat curing temperatures on fly ash-based geopolymer concrete. International Journal of Engineering and Technology, 8(1), 15–19. [Online].

85. Azarsa, P., Gupta, R., Azarsa, P., & Biparva, A. (2021). Durability and self-sealing examination of concretes modified with crystalline waterproofing admixtures. Materials (Basel), 14(21).

86. Luukkonen, T., Abdollahnejad, Z., Yliniemi, J., Kinnunen, P., & Illikainen, M. (2018). One-part alkali-activated materials: A review. Cement and Concrete Research, 103, 21–34.

87. Yener, E. (2020). Curing time and temperature effect on the resistance to wet-dry cycles of fly ash added pumice-based geopolymer. Journal of Cement-Based Composites, 1(2), 19–25.

88. ATİŞ, C. D., ALİ, O. A. A., DURAK, U., İLKENTAPAR, S., & KARAHAN, O. (2020). Strength development of heat-cured and ambient-cured sodium hydroxide activated fly ash-based geopolymer. Dicle Üniversitesi Fen Bilim. Enstitüsü Dergisi, 9(2), 79–88. [Online]. Available: https://dergipark.org.tr/tr/pub/dufed.

89. Bezabih, T., Kanali, C., & Thuo, J. (2023). Effects of teff straw ash on the mechanical and microstructural properties of ambient cured fly ash-based geopolymer mortar for onsite applications. Results in Engineering, 18(March), Article 101123.

90. Shinde, B. H., & Kadam, K. N. (2016). Properties of fly ash-based geopolymer mortar with ambient curing. International Journal of Engineering Research, 8(1), 203–206. [Online]. Available: http://www.ijer.in/ijer/publication/v5si1/48.

91. Moradikhou, S., & Moradikhou, A. B. (2021). Geopolymer concrete based on Class C fly ash cured at ambient condition. Journal of Civil Engineering Materials and Applications, 5(4), 177–195.

92. Liu, J., Shi, X., Zhang, G., & Li, L. (2023). Study the mechanical properties of geopolymer under different curing conditions. Minerals, 13(5).

93. Poloju, K. K., & Srinivasu, K. (2020). Impact of GGBS and strength ratio on mechanical properties of geopolymer concrete under ambient curing and oven curing. Materials Today: Proceedings, 42, 962–968.

94. Nath, P., & Sarker, P. K. (2014). Effect of GGBFS on setting, workability, and early strength properties of fly ash geopolymer concrete cured in ambient condition. Construction and Building Materials, 66, 163–171.

95. Alexander, A. E., & Shashikala, A. P. (2022). Studies on the microstructure and durability characteristics of ambient cured FA-GGBS based geopolymer mortar. Construction and Building Materials, 347, Article 128538.

96. Luan, Y., Wang, J., Ma, T., Wang, S., & Li, C. (2023). Modification mechanism of flue gas desulfurization gypsum on fly ash and ground granulated blast-furnace slag alkali-activated materials: Promoting green cementitious material. Construction and Building Materials, 396, Article 132400.

97. Krishna Rao, A., & Rupesh Kumar, D. (Year). Experimental and microstructural analysis on fly ash-GGBS based geopolymer concrete under ambient curing condition. Title of the Journal, Volume (Issue), Page range.

98. Beig, M. A. (2019). An experimental study on the effect of curing temperature on geopolymer concrete using foundry sand, 1828–1833.

99. Pehlivan, A. O. (2020). Effect of alkali content and activator modulus on mechanical properties of alkali-activated mortars. Karaelmas Journal of Engineering and Science, 10(2), 177–185.

100. Puspita, N., Hani'A, A. I., & Fauzi, M. (2020). The effect of Ground Granulated Blast Furnace Slag (GGBFS) on Portland cement type II to compressive strength of high-quality concrete. IOP Conference Series: Materials Science and Engineering, 830(2). https://doi.org/10.1088/1757-899X/830/2/022068.

101. Saleeh, N.KH. (2022). Investigation of the Effect of Water Reducers on the Slag-Based Alkali-Activated Material. Unpublished civil engineering thesis.

102. Ameri, F., Shoaei, P., Zareei, A. S., Behforouz, B. (2019). Geopolymers vs. alkali-activated materials (AAMs): A comparative study on durability, microstructure, and resistance to elevated temperatures of lightweight mortars. Construction and Building Materials, 222, 49–63.

103. Kovalchuk, O., Kochetov, G., Samchenco, D., Kolodko, A. (2019). Development of a technology for utilizing the electroplating wastes by applying a ferritization method to the alkaline-activated materials. Construction and Architecture, Povitroflotskyi ave., 31, Kyiv, Ukraine, 03037.

104. Collins, F. G., Sanjayan, J. G. (1999). Workability and mechanical properties of alkali-activated slag concrete. Cement and Concrete Research, 29, 455–458.

105. ASTM C109 (Cubes) & ASTM C39 (Cylinders). (n.d.). Testing for Compressive Strength. ASTM International, 109, 2–4.

106. ASTM C230. (2010). Standard Specification for Flow Table for Use in Tests of Hydraulic Cement 1. Annual Book of ASTM Standards, 4–9.

107. Xiao, S., Suleiman, M. T., Al-Khawaja, M. (2019). Investigation of effects of temperature cycles on soil-concrete interface behavior using direct shear tests. Soils and Foundations, 59(5), 1213–1227.

108. Singh, A., Bhadauria, S. S., Thakare, A. A., Kumar, A., Mudgal, M., Chaudhary, S. (2023). Durability assessment of mechanochemically activated geopolymer concrete with a low molarity alkali solution. Journal of Physical Sciences, Elsevier. (Forthcoming).

109. Setlak, K., & Korniejenko, K. (2022). Behavior of geopolymers under changing curing conditions. Journal Name, June, 19171.

110. Dinh, H. L., Doh, J. H., Liu, J., Lu, L., Song, H., & Park, D. (2023). Comprehensive assessment of geopolymer concrete mechanical and environmental

performance with glass cullet fine aggregates. Journal of Building Engineering, 76, Article 107094.

111. Niş, A., & Altundal, M. B. (2023). Durability performance of alkali-activated concretes exposed to sulfuric acid attack. Revista de la Construcción, 22(1), 16–35.

112. Cong, P., & Cheng, Y. (2021). Advances in geopolymer materials: A comprehensive review. Journal of Traffic and Transportation Engineering (English Edition), 8(3), 283–314.

113. Aghabaglou M, A., Özen, S., Altun, M. G., & Faqiri, Z. A. (2020). Effect of water curing temperature on compressive strength development and water absorption capacity of mortar mixtures. Sigma Journal of Engineering and Natural Sciences, 38(1), 135–148.

114. Castillo, H., Collado, H., Droguett, T., Vesely, M., Garrido, P., & Palma, S. (2021). Factors affecting the compressive strength of geopolymers: A review, 1–28.

115. Wong, L. S. (2022). Durability performance of geopolymer concrete: A review. Polymers (Basel), 14(5). https://doi.org/10.3390/polym14050868.

116. Imtiaz, L., Ur Rehman, S. K., Memon, S. A., Khan, M. K., & Javed, M. F. (2020). A review of recent developments and advances in eco-friendly geopolymer concrete. Applied Sciences, 10(21), 1–56.

117. Azarsa, P., & Gupta, R. (2020). Freeze-thaw performance characterization and leachability of potassium-based geopolymer concrete. Journal of Composites Science, 4(2), Article 45.

118. Deventer, J. S. J., Nicolas, R. S., Ismail, I., Bernal, S. A., Brice, D. G., & Provis, J. L. (2014). Microstructure and durability of alkali-activated materials as key parameters for standardization. Journal of Sustainable Cement-Based Materials, 4(2), 116–128.

119. Sruthi, S., & Gayathri, V. (2023). Synthesis and Evaluation of Eco-Friendly, Ambient-Cured, Geopolymer-Based Bricks Using Industrial By-Products. Buildings, 13(2), Article 510

ADDITIONS

ADD #1 – Photos from experimental studies,

Table 1. The breakdown forms patterns and cracks after the compressive strength test for GGBFS and GBFS samples at 60°C

60 °C	For 1 hour	For 2 hours	For 3 hours
GG6_a		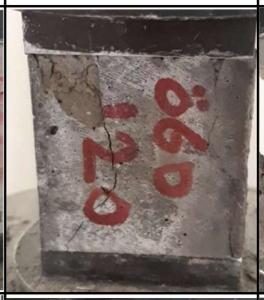	
GG6_w			
60 °C	For 1 hour	For 2 hours	For 3 hours
G6_a			
G6_w			

Table 2. The breakdown forms patterns and cracks after the compressive strength test for GGBFS and GBFS samples at 80°C.

80 °C	For 1 hour	For 2 hours	For 3 hours
G8_a			
G8_w			
80 °C	For 1 hour	For 2 hours	For 3 hours
GG8_a			
GG8_w			

Table 3. The breakdown forms patterns and cracks after the compressive strength test for GGBFS and GBFS samples at 120°C.

120 °C	For 1 hour	For 2 hours	For 3 hours
G12_a			
G12_w	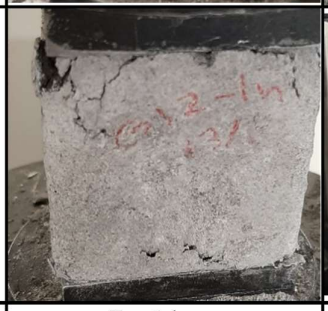		
120 °C	For 1 hour	For 2 hours	For 3 hours
GG12_a			
GG12_w			

Table 4. The breakdown forms patterns and cracks after the compressive strength test for GGBFS and GBFS samples at 140°C.

140 °C	For 1 hour	For 2 hours	For 3 hours
G14_a			
G14_w		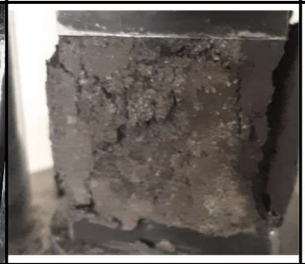	
140 °C	For 1 hour	For 2 hours	For 3 hours
GG14_a			
GG14_w			

Table 5. The breakdown forms patterns and cracks after the compressive strength test for GGBFS and GBFS samples at 160 °C.

160 °C	For 1 hour	For 2 hours	For 3 hours
G16_a			
G16_w			
160 °C	For 1 hour	For 2 hours	For 3 hours
GG16_a			
GG16_w			

Table 6. The breakdown forms patterns and cracks after the compressive strength test for GGBFS and GBFS reference samples.

G-A		GG-A	
G-W	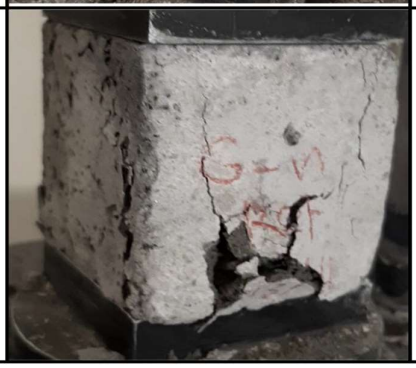	GG-W	

CURRICULUM VITAE

Kinda Ziad ALNAHEEL completed her primary, secondary, and high school education in Homs/Syria. Following this, she embarked on her undergraduate program at AL-Baath University in the Department of Civil Engineering in the academic year 2013/2014, successfully graduating in 2018. Post-graduation, Kinda gained valuable experience by working for two years in Syria as a trainee engineer.

In 2019, She moved to Türkiye and commenced her master's degree in Civil Engineering at Karabük University. This project belongs to her supervisor Assoc. Prof. Dr. İlker TEKİN.